A Reexamination of the Radiative Balance of the Stratosphere

EDUARDO P. OLAGUER, HU YANG, AND KA KIT TUNG

Department of Applied Mathematics, University of Washington, Seattle, Washington

(Manuscript received 25 January 1991, in final form 30 September 1991)

ABSTRACT

Previous diagnostic calculations of the stratospheric radiation budget using observed temperature and absorber distributions produce net heating rates that, although qualitatively similar in their overall patterns, differ quantitatively from each other. Furthermore, when horizontally averaged over the globe, most heating rates reveal significant departures from radiative equilibrium. It is shown that globally averaged infrared cooling and solar heating should theoretically be in balance to within 0.03 K day^{-1} throughout the stratosphere over monthly means and to within smaller ranges over longer time periods. Such accuracies cannot be attained with current methods and available data. Since it is shown here that distributions of important chemical tracers are sensitive to diabatic transport differences larger than 0.1 K day^{-1} in the lower stratosphere, global radiative imbalances should at least be kept to within 0.1 K day^{-1}. This last, less ambitious goal appears to be almost achievable using current technology.

A comprehensive radiative transfer algorithm has been constructed based on accurate and efficient methods for use in coupled stratospheric models of chemistry, dynamics, and radiative transfer. The individual components of our code are validated here against available line-by-line calculations. Compared to line-by-line calculations, the total IR heating has an accuracy of 10% in the stratosphere and the errors are less than 0.07 K day^{-1} in the lower stratosphere. Our result happens to have radiative heating and cooling rates that are globally balanced to about 0.1 K day^{-1} in the lower stratosphere. Furthermore, the net heating rate in the tropical lower stratosphere, which controls the strength of the important Brewer–Dobson circulation, is found to be weaker than previously thought, with important implications for the global distribution of chemical species. In an attempt to explain the differences among existing models, a set of nine case runs is performed with different input datasets of temperature and ozone, with various degrees of degradation of accurate methods and physical parameterizations, and with different numerical implementations. Although it is difficult to perform a true intercomparison of existing models based solely on published material, one finds, based on experiments conducted using our model, that some commonly adopted approximations in IR schemes and physical parameterizations tend generally to increase the tropical net heating in the lower stratosphere by over a factor of 2 and also to significantly increase the global radiative imbalance at other heights.

1. Introduction

Recent work in middle-atmospheric modeling has emphasized the computation of accurate diabatic heating rates in deriving the meridional transport circulation in the stratosphere (Solomon et al. 1986; Callis et al. 1987; Gille et al. 1987; Rosenfield et al. 1987). While these are more accurate compared to Newtonian cooling parameterizations, there are significant differences in radiative heating rates generated by modern-day codes, differences that are attributable to the varying levels of physical approximation employed by specific authors.

Modern radiative codes have several features, each with its own peculiar set of conceptual and numerical complications. These features include the treatment of infrared (IR) or longwave cooling, solar or shortwave heating, and cloudiness. A general survey of theoretical methods employed for each of these features is provided by Stephens (1984).

With respect to infrared radiation, the most critical aspects of a radiative transfer algorithm are its resolution in the IR spectrum and corresponding treatment of absorption line properties. Infrared codes range in complexity from the rigorous, but computationally demanding, line-by-line (LBL) models (e.g., Fels and Schwarzkopf 1981; Schwarzkopf and Fels 1985) to highly efficient, but parameterized, broadband schemes (e.g., Rodgers 1968; Ramanathan 1976; Ou and Liou 1983). In between these two extremes are the so-called narrowband random models (e.g., Wehrbein and Leovy 1982; Kiehl and Solomon 1986), which employ a statistical treatment of absorption line parameters within narrow spectral segments. Generally speaking, IR algorithms employed for prediction (as opposed to diagnostic) studies sacrifice accuracy for computational efficiency, since radiative heating rates must be continually updated.

Corresponding author address: Prof. Ka Kit Tung, University of Washington, Department of Applied Mathematics FS-20, Seattle, WA 98195.

In the case of solar radiation, the methods for treating atmospheric absorption are far more straightforward. However, the inclusion of the effects of multiple scattering poses difficulties, with respect to both the underlying method to be used (see King and Harshvardhan 1986) and also the nature and distribution of the scatterers, primarily clouds. Since clouds also affect the exchange of infrared radiation, a thorough evaluation of their role is important in any definitive study of the radiative budget of the middle atmosphere.

Several diagnostic studies of the stratospheric radiation field have been presented in the literature within recent years. Broadband models were used by Gille and Lyjak (1986), Callis et al. (1987), and Pawson and Harwood (1989) to compute seasonal and monthly mean net radiative heating rates based on observationally derived distributions of atmospheric absorber and temperature, mostly from Limb Infrared Monitor of the Stratosphere (LIMS) data. Rosenfield et al. (1987) employed broadband methods with SBUV and SME ozone data and NMC temperatures. Kiehl and Solomon (1986) used a narrowband Fels–Malkmus model (Fels 1979) together with LIMS satellite observations in their radiative calculations. While the gross patterns of net heating presented in these diagnostic studies are in general agreement, it is difficult to assess the actual differences in magnitude among the various results. Where these differences matter most, and where the contours presented by these authors are sparsest in detail, is in the lower stratosphere, particularly near the equator. Interestingly, chemical tracer models employing diabatic circulations derived from these different heating fields have yielded rather different concentrations globally.

Callis et al. (1987), using diabatic circulation trajectories, showed that middle to upper stratospheric air parcels tend to originate near the equatorial tropopause. Haigh (1984), upon whose radiative algorithm the calculations of Pawson and Harwood (1989) are based, noted that ozone column amounts everywhere are very sensitive to the magnitude of the heating in the equatorial lower stratosphere. This fact was also pointed out by Jackman et al. (1989), who experimented with different sets of fixed diabatic heating rates within a two-dimensional model with coupled dynamics and chemistry. Unlike Jackman et al., however, Haigh employed a fully coupled radiative–dynamical–chemical model and found that column ozone was substantially influenced by the complex interaction among ozone, temperature, and the radiative forcing.

The conclusions of Haigh (1984) and Jackman et al. (1989) are not surprising, since it is the upward, poleward, and downward "Brewer–Dobson" circulation that determines the global balance between ozone production (which dominates loss near the tropopause at low latitudes) and ozone loss (which dominates production at high latitudes in the lower stratosphere; see Jackman et al. 1986). The strength of this circulation, in turn, is approximately proportional to the diabatic heating (Dunkerton 1978; Tung 1982).

Because the equatorial lower stratosphere is very close to radiative equilibrium, changes in the diabatic heating of only a few tenths of a degree kelvin per day in this vicinity can have a significant impact on the distribution of trace chemical species throughout the globe. There are several sources of uncertainty that can produce errors of this magnitude within a diagnostic or prognostic model. Most obvious are errors resulting from the physical and numerical approximations adopted within the radiative transfer algorithm. Crisp (1989) compared infrared heating rates generated by several broadband algorithms employed by different 2D stratospheric models with results from the GFDL line-by-line (LBL) code (Fels and Schwarzkopf 1981; Schwarzkopf and Fels 1985). The deviations from the LBL heating rates were of the order of 20%–30% in the lower stratosphere, with errors as high as 80% for ozone IR heating.

Other errors can result from the neglect of such physical processes as multiple scattering and reflection of radiation by cloud decks. The diabatic heating calculations presented by Kiehl and Solomon (1986) and Rosenfield et al. (1987) do in fact ignore these processes, and they estimate that the net heating in the lower stratosphere can be altered by one to a few tenths of a degree per day due to cloudiness.

Still other errors are the result of uncertainties in observations or model predictions of temperature and of stratospheric absorbers such as water vapor and ozone, which are required as input to the radiative algorithm. Diagnostic studies based on LIMS satellite observations, for instance, tend to compute a horizontally averaged net radiative heating in the lower mesosphere that is substantially nonzero, owing possibly to the underestimate of temperatures above 1 mb by the LIMS instrument (Gille and Lyjak 1986).

The primary objective of the present study is to reexamine the radiative balance of the stratosphere in the light of the possible sensitivity of tracers to small changes in the diabatic heating. A secondary objective of ours is to provide a radiation code that is not only sufficiently comprehensive and accurate, but also fast enough to be incorporated in coupled models of the stratosphere requiring frequent computation of radiative heating rates. The issue of accuracy is addressed here by comparison with available line-by-line calculations. Lastly, we shall compare the results of different approximations commonly employed in radiative transfer algorithms and evaluate their effects on tracer transport with the aid of a two-dimensional ozone model.

2. Global balance requirement

It is generally thought that atmospheric infrared cooling and solar heating rates should be in balance over climatological time scales when horizontally av-

eraged over the globe. It turns out, however, that no rigorous derivation of such a condition exists. In fact, when such an average is taken on isobaric surfaces, as is normally done, the globally averaged net heating rate is not required to be zero by the equations governing energy and mass.

Let T be the temperature, $\theta = T(p_{00}/p)^{R/c_p}$ the potential temperature, and Q the net diabatic heating rate in kelvin per second. The thermodynamic equation is

$$\frac{d}{dt}\ln\theta = \frac{Q}{T}, \tag{1}$$

where d/dt is the three-dimensional substantial derivative. In pressure coordinates, Eq. (1) can be rewritten as

$$\frac{\partial}{\partial t}T + \frac{\partial}{\partial x}(uT) + \frac{\partial}{\partial y}(v\cos\phi T) + \frac{1}{\rho_0}\frac{\partial}{\partial z}(\rho_0 wT) + \frac{g}{c_p}w = Q, \tag{2}$$

where the continuity equation is used in the form

$$\frac{\partial}{\partial x}(\rho_0 u) + \frac{\partial}{\partial y}(\rho_0 v\cos\phi) + \frac{\partial}{\partial z}(\rho_0 w) = 0 \tag{3}$$

[$dx = a\cos\phi d\lambda$, $y = a\sin\phi$, $z = H\ln(p_0/p)$, a = radius of earth, ϕ = latitude, λ = longitude, $H = 7$ km, p_0 = surface pressure, p = pressure and $\rho_0(z) = \rho_0(0)\exp(-z/H)$].

Let $\langle\ \rangle_p$ denote a horizontal average over constant pressure surfaces. Applying this operator to the thermodynamic equation and employing the boundary condition $v\cos\phi = 0$ at the poles, we obtain

$$\frac{\partial}{\partial t}\langle T\rangle_p + \frac{1}{\rho_0}\frac{\partial}{\partial z}[\rho_0\langle wT\rangle_p] + \frac{g}{c_p}\langle w\rangle_p = \langle Q\rangle_p. \tag{4}$$

Horizontally averaging Eq. (3), we have $\partial(\rho_0\langle w\rangle_p)/\partial z = 0$, which, upon integration and application of the boundary condition $\rho_0\langle w\rangle_p = 0$ at infinity, yields

$$\langle w\rangle_p \equiv 0. \tag{5}$$

Equation (4) then becomes

$$\frac{\partial}{\partial t}\langle T\rangle_p + \frac{1}{\rho_0}\frac{\partial}{\partial z}(\rho_0\langle wT\rangle_p) = \langle Q\rangle_p. \tag{6}$$

No further progress can be made concerning the balance of Q, unless approximations are made.

In practice, most chemical transport models formulated in pressure coordinates do not use the exact energy equation (2). An approximation often adopted involves the neglect of the nonlinear temperature advection terms when applied to the temperature deviation from the horizontally averaged temperature, $T_0(z)$. Under such an approximation, Eq. (4) is replaced by

$$\frac{\partial}{\partial t}\langle T\rangle_p + \Gamma\langle w\rangle_p = \langle Q\rangle_p, \tag{7}$$

where $\Gamma = g/c_p + dT_0(z)/dz$. Equation (7), together with Eq. (5), implies that the globally integrated heating rate should vanish when averaged over time (assuming no global temperature change over time or steady-state condition), that is,

$$\langle Q\rangle_p = 0.$$

This result hinges on the approximation of neglecting the vertical heat flux term associated with temperature deviation from $T_0(z)$ in Eq. (2) as compared to terms retained, which is questionable in the present context. Nevertheless, in models adopting such an approximate energy equation in pressure coordinates, consistency requires that Q be globally balanced. Failure to do so will violate mass conservation. Therefore, in most 2D models, the computed imbalance is generally uniformly subtracted away from the local heating rate, an ad hoc procedure, introducing a further source of uncertainty and error.

A better theoretical global balance requirement can be obtained when the horizontal average is performed on surfaces of constant potential temperature (see Tung 1982, 1986; Yang et al. 1990, 1991, for the relevant formulation in isentropic coordinates). Using

$$z_1 = \kappa^{-1}H\ln(\theta/\theta_0) \tag{8}$$

as the vertical coordinate ($\kappa = R/c_p$, $\theta_0 = 263$ K) and $w_1 = dz_1/dt$ as the vertical velocity in this isentropic coordinate system, the thermodynamic equation can simply be written as

$$w_1 = \frac{H}{\kappa T}Q \tag{9}$$

and the continuity equation as

$$\frac{\partial}{\partial t}\sigma + \frac{\partial}{\partial x}\sigma u + \frac{\partial}{\partial y}\sigma v\cos\phi + \frac{\partial}{\partial z_1}\sigma w_1 = 0, \tag{10}$$

where $\sigma = \rho\partial z/\partial z_1$ is the "density" in isentropic coordinates (z here is the geometric altitude). If we denote horizontal averages on isentropic surfaces by $\langle\ \rangle_\theta$ and globally average Eq. (10), then

$$\frac{\partial}{\partial t}\langle\sigma\rangle_\theta + \frac{\partial}{\partial z_1}\langle\sigma w_1\rangle_\theta = 0. \tag{11}$$

Employing the hydrostatic relationship

$$\sigma = -\frac{1}{g}\frac{\partial p}{\partial z_1} \tag{12}$$

and the upper boundary condition at infinity, one obtains from Eq. (11)

$$\langle\sigma w_1\rangle_\theta = \frac{1}{g}\left\langle\frac{\partial p}{\partial t}\right\rangle_\theta. \tag{13}$$

Finally, if we define the weighted horizontally average net diabatic heating in isentropic coordinates as

$$\hat{Q} \equiv \frac{\langle \sigma Q/T \rangle_\theta}{\langle \sigma/T \rangle_\theta}, \tag{14}$$

then from Eq. (9) the result is

$$\hat{Q} = \frac{\kappa}{gH} \frac{\langle \partial p/\partial t \rangle_\theta}{\langle \sigma/T \rangle_\theta}. \tag{15}$$

Thus, the weighted horizontal average net diabatic heating in isentropic coordinates should vanish under steady-state assumption and is in any case small when averaged in time over a sufficiently long period.

Given the uncertainties involved in the radiative computation and observation, we do not expect that evaluating the left-hand side of Eq. (15) through a calculation of Q and then globally averaging the result will yield the same value as by evaluating the right-hand side from a time-series of temperature data. Instead, the right-hand side of Eq. (15) should be treated as a "theoretical balance requirement" for globally integrated net radiative heating rate. In the past, this requirement has been presumed to be zero.

We have evaluated this theoretical constraint using three-dimensional NMC temperature data supplied to us by D. Wu and E. Nash of NASA. Pressure is related to temperature through the relation

$$p = p_0 \left(\frac{T}{\theta} \right)^{1/\kappa}. \tag{16}$$

We first sort the temperature data onto surfaces of constant θ, and then perform horizontal averages. To eliminate transients, the 3D daily temperature is Fourier analyzed into 72 time harmonics for data of every year. Thus, transients with periods shorter than 5 days have been filtered out.

Before actual numbers are presented, it is perhaps instructive to examine first the variability of the globally averaged temperature to gain some familiarity with the order of magnitude of the right-hand side of Eq. (15). It can be shown that the latter is proportional to the time derivative of the temperature field globally averaged on surfaces of constant potential temperature, that is,

$$\hat{Q} \propto \frac{\partial}{\partial t} \langle T \rangle_\theta. \tag{17}$$

The "constant" of proportionality is approximately 1 using appropriate parameters for the stratosphere.

In Figure 1, the annual mean of $\langle T \rangle_\theta$ for 1980 is shown as a function of z_1 and the deviation from it as a function of time and z_1. Note the vertical coordinate z_1 is potential temperature in logarithmic scale, as defined by (8). The corresponding potential temperature and pressure levels calculated using the globally and annually averaged temperature shown here are listed in Table 1. Figure 1 showed that the globally integrated temperature field varies in a very tight range. The globally integrated temperature seldom deviates from its annual mean by more than 1 K. This feature is typical for other years as well, although some years may show slight data discontinuity in time, which is to be expected for this operational dataset. When this happens, $\langle T \rangle_\theta$ may show a deviation from its annual mean by as much as 5 K in the upper stratosphere.

Taking 1 K as a typical temperature deviation, we find that the right-hand side of (17) is about 0.03 K

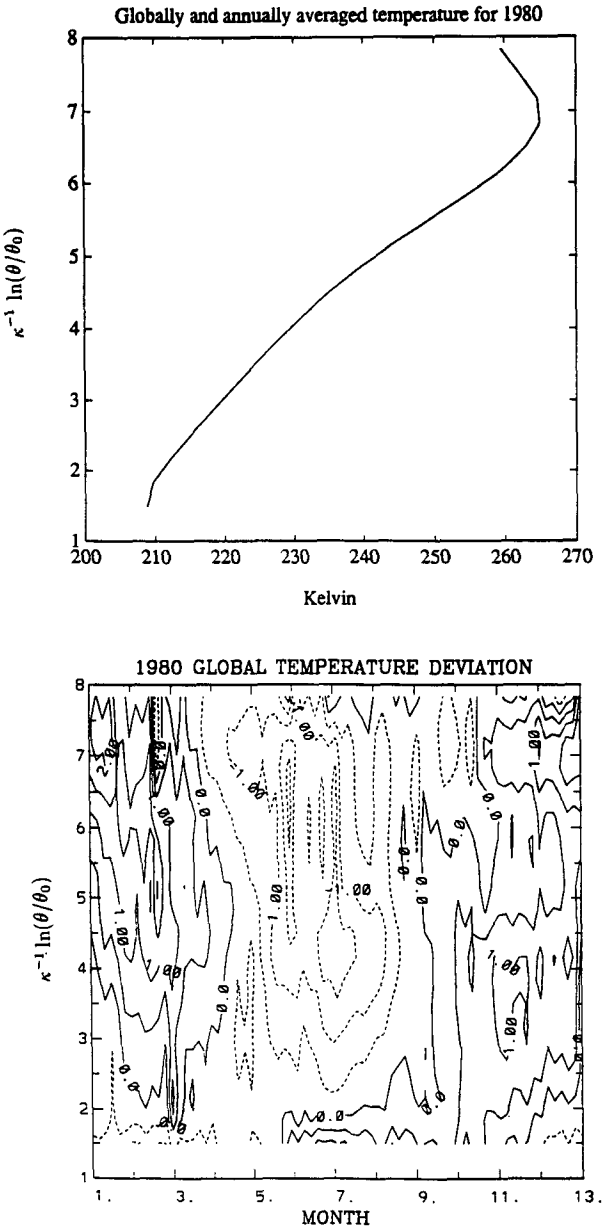

FIG. 1. Globally averaged NMC temperature for 1980 in isentropic coordinate: (a) annual mean; (b) deviation from annual mean.

TABLE 1. Monthly averaged global heating rate constraint for $\hat{Q}$ for January, April, July, and October 1980 calculated by right-hand side of Eq. (15) (last four columns, in unit of 10^{-2} K day^{-1}). The first two columns list the vertical coordinate z_1/H and the corresponding potential temperature values. The approximate pressure levels shown in column four are calculated by using the globally and annually averaged temperature for 1980 shown in column three and also in Fig. 1a.

z_1/H	θ (K)	T (K)	p (mb)	Jan	Apr	Jul	Oct
7.833	2466	259.49	0.38	−1.90	1.62	−0.01	−0.19
7.500	2242	262.13	0.55	−1.71	1.03	0.38	−0.86
7.167	2038	264.64	0.79	−1.32	0.42	0.73	−1.38
6.833	1853	265.01	1.11	−0.90	−0.36	0.72	−1.39
6.500	1685	262.95	1.50	−0.49	−1.20	0.25	−0.02
6.167	1532	259.54	2.00	0.15	−1.75	0.00	1.20
5.833	1392	254.70	2.62	1.03	−1.92	0.00	1.98
5.500	1266	249.41	3.39	1.27	−2.03	−0.17	2.68
5.167	1151	244.19	4.40	0.90	−2.17	−0.74	3.22
4.833	1046	239.40	5.73	1.00	−2.65	−1.14	2.39
4.500	951	235.12	7.51	1.82	−3.36	−0.83	1.08
4.167	865	231.16	9.87	2.06	−3.68	−0.35	0.53
3.833	786	227.62	13.05	1.65	−3.42	0.06	0.49
3.500	715	224.36	17.32	1.18	−3.16	0.44	0.39
3.167	650	221.18	22.99	0.63	−2.68	1.03	0.61
2.833	591	218.05	30.52	−0.01	−2.28	1.20	0.71
2.500	537	215.05	40.58	−0.43	−2.09	1.11	0.57
2.167	488	212.15	54.01	−0.63	−1.65	0.54	0.54
1.833	444	209.68	72.34	−1.48	−0.11	−0.77	1.66
1.500	404	208.80	99.48	−1.36	3.25	−3.89	1.49

day^{-1} over a month. Therefore, the monthly time mean of globally averaged net radiative heating rate imbalance should be constrained by a small number on the order of 0.03 K day^{-1}. Shorter or longer time averages of $\hat{Q}$ will yield larger or smaller imbalances in inverse proportion to the averaging period (provided that the latter is longer than 5 days).

Calculation using the exact expression on the right-hand side of Eq. (15) instead of (17) yields Table 1, which shows that the imbalance, $\hat{Q}$, when averaged over a month, is largely within 0.03 K day^{-1} throughout the stratosphere for all of the four months (January, April, July, and October 1980) that we examined.

Table 1 shows that our atmosphere is remarkably well balanced in its global radiative heating and cooling. Note that there is no such balance requirement for instantaneous values of heating and cooling, but over monthly means the atmosphere should be balanced within 0.03 K day^{-1} when averaged globally on surfaces of constant potential temperature.

In practice, when Q is calculated from radiative transfer codes now available, the "theoretical" balance apparent in Table 1 cannot be achieved. Imbalances as large as 1 K day^{-1} have previously been reported. It was not clear if these were caused by problems with input temperature and absorber distribution data, with missing absorbers, or with a lack of accuracy in the radiative codes. We cannot resolve these issues unambiguously with current technology. Nevertheless, we can show that large imbalance in radiative heating and cooling is *not* a systematic and common deficiency of all radiative codes. With a judicious choice of radiative transfer methods (chosen based on the basis of their accuracy, not on the basis of balance requirement), the imbalance turns out to be largely within 0.1 K day^{-1} in the lower stratosphere. This then provides us with an opportunity to discuss and offer a partial explanation of how the large imbalances were previously obtained in some models.

3. The radiative transfer algorithm

a. *Infrared radiation*

The atmospheric absorbers accounted for in the infrared code are carbon dioxide, ozone, water vapor, methane, and nitrous oxide. The following subsections detail the physical and numerical approximations used to calculate the infrared heating due to each of these absorbers.

1) CARBON DIOXIDE

The CO_2 IR code utilizes the simplified exchange approximation of Fels and Schwarzkopf (1975), wherein the cooling-to-space contribution is computed accurately from a random model, while the atmospheric layer exchange terms are calculated using a more empirical broadband emissivity parameterization. The advantage of this method is that for carbon dioxide cooling to space dominates layer exchange, so that the larger relative errors found using the pure broadband scheme affect only a small portion of the total infrared heating by CO_2. Moreover, unlike purely parametric schemes such as that of Harshvardhan et al. (1987), this approach is applicable to climatic regimes that differ significantly from that of the current atmosphere, since the leading-order term is tied to actual absorption line properties.

The emissivity parameterization is taken from Ou and Liou (1983) and is based on a polynomial fit to the LBL calculations of Fels and Schwarzkopf (1981). Although Ou and Liou claimed errors of less than 5% for their parameterization, we found that when we applied it to compute both the cooling-to-space and layer exchange terms using the revised standard grid of Schwarzkopf and Fels (1985), the errors increased to about 20% throughout most of the stratosphere. This is not surprising, since Schwarzkopf and Fels (1985) themselves found fractional errors of up to 30% when they applied an analytical fit to their calculated absorptances directly to compute absorptances on the old grid of Fels and Schwarzkopf (1981).

For the cooling-to-space calculation, the wavenumber interval from 450 to 900 cm^{-1} is divided into N subintervals of uniform width $\Delta\nu$. Within each sub-

interval, the total Voigt absorptance A_v is computed from the empirical interpolation formula of Rodgers and Williams (1974), as was suggested by Crisp et al. (1986). Thus,

$$A_V^2 = A_L^2 + A_D^2 - (A_L A_D / A_W)^2, \quad (18)$$

where A_L, A_D, and A_W are the absorptances in the pure Lorentz, pure Doppler, and weak limits, respectively.

The Lorentz line halfwidth is assumed to depend on pressure p and temperature T as follows:

$$\alpha_L(p, T) = \alpha_L(1 \text{ atm}, 250 \text{ K})\left(\frac{p}{1 \text{ atm}}\right)\left(\frac{250 \text{ K}}{T}\right)^{\gamma}, \quad (19)$$

where the exponent γ depends on the absorber and is set equal to 0.75 in the case of carbon dioxide. For a given spectral interval with mean line spacing δ (cm^{-1}), the average Lorentz halfwidth is computed from

$$\frac{\pi \alpha_L}{\delta} = \frac{4}{\Delta \nu} \frac{(\sum \sqrt{S_i \alpha_{L,i}})^2}{\sum S_i}, \quad (20)$$

where S_i denotes the strength of the ith line.

The absorptance in the pure Doppler limit is calculated by assuming, as did Fels (1979), that the Doppler line shape is rectangular, with a halfwidth given by

$$\nu_0 = \beta(\nu/c)(2BT/\mu)^{1/2}, \quad (21)$$

where β is an adjustable parameter of order unity, ν is the mean wavenumber, c is the speed of light, B is Boltzmann's constant, and μ is the CO_2 molecular mass. The value of β was chosen to be 1.0 for pressures less than 1 mb and 0.5 for pressures greater than 1 mb, as this gave the best fit to LBL calculations.

The absorptance in the weak limit is simply

$$A_W = \bar{m} \sum S_i(250 \text{ K}), \quad (22)$$

where the weighted absorber amount in the Curtis–Godson approximation (Rodgers and Walshaw 1966) is given in terms of the actual amount m by

$$\bar{m} = 1.66 \int \Phi dm, \quad (23)$$

$$\Phi = \frac{\sum S_i(T)}{\sum S_i(250 \text{ K})} \approx a(T - 250 \text{ K}) + b(T - 250 \text{ K})^2, \quad (24)$$

where the parameters a and b are an empirical fit to the actual temperature dependence of the line strengths. Note also that the diffusivity approximation has been used in performing the vertical integration in the expression for the weighted absorber amount.

To derive the Lorentz and Doppler absorptances, we use two distinct random models for different altitude regions. The first applies to pressures greater than 1 mb, while the second applies to all other levels. The reason for this is that the radiative calculation is far more sensitive to the assumed line-strength distribution than to the spectral resolution at low pressures (see Crisp et al. 1986). Below the 1-mb pressure level, a Malkmus (1967) model with $N = 90$ ($\Delta\nu = 5$ cm^{-1}) is used. The probability distribution for the line strengths (normalized to the number of lines) is then given by

$$P(S) = \frac{\Delta \nu}{S\delta} e^{-S/k}, \quad \frac{k}{\delta} = \frac{\sum S_i(250 \text{ K})}{\Delta \nu}, \quad (25)$$

where the quantity κ is the mean line strength in an interval of width $\Delta\nu$. The transmission functions for the pure Lorentz and pure Doppler limits can now be written, respectively, as (Fels 1979)

$$T_L = \exp\left\{-\frac{\pi \alpha_L}{2\delta}\left[\left(1 + \frac{4k\bar{m}}{\pi \alpha_L}\right)^{1/2} - 1\right]\right\}, \quad (26)$$

$$T_D = \left(1 + \frac{2k\bar{m}}{\nu_0}\right)^{-\nu_0/2\delta}, \quad (27)$$

where the line widths are weighted with respect to absorber amount as follows:

$$\alpha_L = \frac{\int \alpha_L(p, T) d\bar{m}}{\bar{m}}, \quad \nu_0 = \frac{\int \nu_0(T) d\bar{m}}{\bar{m}}. \quad (28)$$

Above the 1-mb level we use a single wavenumber interval of width 450 cm^{-1} and the line strength distribution suggested by Crisp et al. (1986):

$$P(S) = \frac{\Delta \nu}{\delta} \frac{e^{-S/k}}{k} + \frac{\Delta \nu}{\epsilon} \frac{l^{1/4}}{\Gamma(3/4)} S^{-5/4} e^{-S/l}. \quad (29)$$

The first and second components of $P(S)$ represent the distributions of strong ($S > 10$ cm g^{-1}) and weak ($S < 10$ cm g^{-1}) lines, respectively, in the entire 15-micron band. The parameters κ and δ are analogous to the similarly designated quantities used in the Malkmus model, except that they apply only to the strong lines. Similarly, l and ϵ refer to the mean weak line strength and mean weak line spacing, respectively. These quantities, except for ϵ, are derived from the HITRAN database tape (Rothman et al. 1987) and have the following values: $\kappa = 379.6$ cm g^{-1}, $l = 0.0794$ cm g^{-1}, $\delta = 1.393$ cm^{-1}, and $\epsilon = 0.05014$ cm^{-1}.

We note that our expression for the probability distribution Eq. (29) differs from that recommended in Crisp et al. (1986) because we used a different strong line cutoff and normalization method.

We now write the transmission functions for the Lorentz and Doppler limits for the probability distribution (29). These are given by

$$T_L = \exp\left\{-\frac{km_s}{\delta}\left(1+\frac{km_s}{\pi\alpha_L}\right)^{-1/2} - \frac{lm_w}{\epsilon}\right\}, \quad (30)$$

$$T_D = \exp\left\{\frac{km_s}{\delta}\left(1+\frac{km_s}{2\nu_0}\right)^{-1} - \frac{8\nu_0}{\epsilon}\left[\left(1+\frac{lm_w}{2\nu_0}\right)^{1/4} - 1\right]\right\}, \quad (31)$$

where the quantities m_s and m_w are the Curtis–Godson weighted absorber amounts for the strong and weak lines, respectively. In deriving Eq. (30), the weak approximation for the weak lines is used in order to arrive at the simple expression for the Lorentz transmission. This is somewhat different from the method proposed by Crisp et al. (1986), who employed a separate exponential wideband model to calculate the Lorentz absorptance at low pressures.

Once the transmission functions T_L and T_D are known, the corresponding absorptances A_L and A_D can then be found from the expressions:

$$A_L = (1 - T_L)\Delta\nu, \quad A_D = (1 - T_D)\Delta\nu. \quad (32)$$

The cooling-to-space contribution to the CO_2 infrared heating can then be calculated from the total Voigt absorptance as follows:

$$Q_{\mathrm{CTS}} = -\frac{\pi g}{c_p}\sum_{\nu=1}^{N} B_\nu(T)\frac{\partial A_{V,\nu}}{\partial p}, \quad (33)$$

where g is the acceleration due to gravity, c_p is the specific heat at constant pressure, and B_ν is the Planck function.

To avoid vertical discontinuities in the heating due to the use of disparate methods to compute the cooling-to-space term, the CO_2 net infrared heating field is smoothed in the vicinity of 1 mb. Let the pressure level number just above the 1-mb surface be denoted by J and that of the level just below 1 mb by $J + 1$; tildes denote the smoothed field. Then the adjusted infrared heating by carbon dioxide is computed according to the formulas:

$$\tilde{Q}_J = 0.4Q_{J-1} + 0.3Q_J + 0.2Q_{J+1} + 0.1Q_{J+2}, \quad (34)$$

$$\tilde{Q}_{J+1} = 0.4Q_{J+2} + 0.3Q_{J+1} + 0.2Q_J + 0.1Q_{J-1}. \quad (35)$$

The integrals required for the calculation of all heating rates are computed using the trapezoidal rule. Moreover, first derivatives with respect to pressure of either emissivity or absorptance are evaluated analytically in order to reduce sensitivity to the vertical resolution. This is facilitated by our avoidance of cumbersome formulas for the various transmission functions, which in the case of CO_2 is due to the use of simple limits for the line shapes and the algebraic interpolation scheme of Rodgers and Williams (1974). Unlike the single complex expressions for either the Voigt transmission or absorptance found in Fels (1979) and Zhu (1988), our method for calculating the CO_2 absorptance has the virtue of requiring a smaller number of transcendental functions, thus speeding up the computation significantly. Because finite differences are avoided wherever possible, radiative fluxes are generally not computed in our algorithm, although the code could easily be modified to provide this information.

It should be noted that the emissivity evaluated at level i due to thermal emission from level j has a first derivative that is discontinuous at i whenever $i = j$. The CO_2 infrared algorithm normally sets this derivative to zero for such "diagonal" elements. This simplification does not lead to significant errors at most levels, except near the temperature minimum at the tropical tropopause. In this case, the simplification underestimates the heating at the center of a layer due to the differences in temperature at the top and bottom of the layer. To avoid errors of the order of 0.1 K day^{-1} near the tropopause, the missing exchange terms are calculated explicitly using a pure Lorentz narrowband model with Malkmus line strength distribution. The emissivity parameterization of Ou and Liou (1983) is not used for this purpose because the empirical fit is inaccurate for small path lengths near the tropopause. The user of the radiative code has the option of specifying the levels at which the emissivity correction is applied. In the present study, this correction is applied at tropopause only, except for the low-resolution cases in which it is applied at all levels below 0.2 mb.

2) OZONE

The O_3 infrared algorithm is based on the parameterization of Rosenfield (1991). Rosenfield's parameterization is an empirical fit to LBL results using the functional form of the Goody (1952) random models for the center (1020–1055 cm^{-1}) and wings (980–1020 cm^{-1} and 1055–1100 cm^{-1}) of the ozone 9.6-micron band. The transmission function, using Rosenfield's notation, is given by

$$T = \exp\left\{-1.66Su\delta^{-1}\left(1+\frac{Su}{\pi b}\right)^{-1/2}\right\}, \quad (36)$$

where u is the absorber amount, $\delta = 0.1$ cm^{-1} and the parameters S and b are derived from Tables 2 and 3. Unlike Rosenfield (1991), we treat vertical inhomogeneity using the strict Curtis–Godson approximation. We found that this absorption-path scaling method, together with analytic differentiation of Rosenfield's

TABLE 2. The parameter S (cm^{-2} atm^{-1}).

Temperature	Band center	Band wing
200 K	.920	.150
250 K	.885	.205
300 K	.805	.252

TABLE 3. The parameter b (cm^{-1}).

Pressure	Band center	Band wing
0.25 mb	.000471	.000220
1.00 mb	.000534	.000275
2.51 mb	.000691	.000393
10.0 mb	.001730	.000864
25.1 mb	.003930	.001570
100. mb	.012600	.003930
251. mb	.027500	.005500
1000 mb	.055000	.007070

empirical expression for the transmission function, gives results in better agreement with LBL calculations, especially for a tropical atmosphere, than those reported by Rosenfield (1991).

Heating due to the 14-micron band of ozone is not included in our model. Schwarzkopf and Fels (1991) have demonstrated that the effects of this band are completely obscured by line overlap with the 15-micron band of carbon dioxide.

3) WATER VAPOR

The water vapor scheme, like that for carbon dioxide, employs different methods for the upper and lower atmosphere. Below the 10-mb pressure level, we use the nonisothermal emissivity formulation of Ramanathan and Downey (1986) for the pure rotation (0–100 cm^{-1}) and vibration-rotation (1200–2200 cm^{-1}) bands. The two continuum bands (8.3–12.5 μm and 16.7–20.83 μm) are also included, but since these are important only near the surface, the simpler isothermal emissivity scheme of Ramanathan (1976), modified to account for the temperature dependence of the continuum absorption coefficient (Roberts et al. 1976), has been employed in this case. Our expressions for the two continuum emissivities (which Ramanathan denoted by E_2 and E_3) are as follows:

$$E_2 = [0.272 + 8.761^{-4}(T - 300\ \mathrm{K})] \times [1 - \exp\{-20(Y + 0.002Z)\}], \quad (37)$$

$$E_3 = [0.124 + 4.291^{-4}(T - 300\ \mathrm{K})] \times [1 - \exp\{-90(Y + 0.02Z)\}], \quad (38)$$

$$Y = \int \exp\left\{\frac{1800\ \mathrm{K}}{T} - \frac{1800\ \mathrm{K}}{296\ \mathrm{K}}\right\} edW, \quad Z = \int pdW, \quad (39)$$

where the quantities e and W represent the water vapor partial pressure and absorber amount, respectively.

Above 10 mb, we again resort to the simplified exchange approximation. This was necessary in order to properly account for Doppler broadening, which becomes important in the vicinity of 2 mb (Rodgers and Walshaw 1966). The infrared heating at these pressures is calculated only for the pure rotation band. A random model for water vapor cooling-to-space, similar to that for carbon dioxide below 1 mb, is employed, whereas an isothermal emissivity scheme is used to compute infrared heating due to layer exchange. The spectral resolution of the random model is 5 cm^{-1}, while the line-width parameters β and γ are assigned the values 1.0 and 0.64, respectively.

Since the emissivity formulation of Ramanathan and Downey (1986) was fit to narrowband results at pressure greater than 10 mb, a different emissivity scheme is used at lower pressures based on the nonoverlapping strong line limit (Houghton 1977). In this approximation the isothermal emissivity between two levels i and j can be written as

$$\epsilon_{ij} = \frac{\pi \Delta\nu}{\sigma T_j^4} \sum_{\nu} \frac{\sqrt{\pi k_\nu \alpha_\nu}}{\delta_\nu} B_\nu(T) \left(\int_{m_i}^{m_j} pdm \right)^{1/2}, \quad (40)$$

where m is the absorber amount, j is the emitting level, and the summation is over the lines of the pure rotation band. The line parameters within the summation are evaluated at the emitting temperature T_j. The smoothing technique described by Eqs. (34) and (35) is applied to the total water-vapor infrared heating near 10 mb.

The effect of line overlap between water vapor and carbon dioxide is incorporated by multiplying the emissivity derivative of CO_2 by the transmission of water vapor at 15 μm. The latter quantity is computed from a single-interval Goody random model as in Rodgers (1967). Line overlap between water vapor and ozone in the 9.6-micron band is accounted for by multiplying the ozone absorptance derivative by the water vapor transmission function of Roberts et al. (1976) evaluated at the band center.

4) METHANE AND NITROUS OXIDE

Band models for methane near 1306 cm^{-1} and for nitrous oxide near 1285 cm^{-1} are taken from Donner and Ramanathan (1980). The band intensity adopted for methane is 128 cm^{-2} atm^{-1} (Cess et al. 1986), while that of nitrous oxide is taken to be 218 cm^{-2} atm^{-1} (WMO 1982). For simplicity, we ignore line overlap between these two absorbers, as well as any overlap with the continuum bands of water vapor.

b. Solar radiation and cloudiness

The solar radiation code allows for radiative absorption at ultraviolet and visible wavelengths by ozone, molecular oxygen, and nitrogen dioxide and at near-infrared wavelengths by water vapor and carbon dioxide.

The absorption of solar radiation by O_3, O_2, and NO_2 is computed by determining the transmission in narrow spectral intervals using the wavenumber intervals and photon fluxes specified in WMO (1986) (the

coarser of the two recommended grids is employed for wavenumbers beyond 400 nm). Also taken from WMO (1986) are cross sections for ozone absorption, Rayleigh single scattering, and the O_2 Herzberg continuum. The O_2 Schumann–Runge cross sections, however, are computed from the parameterization of Allen and Frederick (1982), while absorption cross sections for NO_2 are from JPL (1987).

Near-infrared absorption above the troposphere is calculated using the empirical expression of Lacis and Hansen (1974) for the water vapor absorptivity and that of Sasamori et al. (1972) for the carbon dioxide absorptivity. Kiehl et al. (1987) found that the latter yields results that agree very well with those generated by the newer absorptance formulation of Kiehl et al. (1985) at pressure levels below 10 mb. Near-infrared heating by CO_2, although negligible at most altitudes in comparison to ozone heating at ultraviolet and visible wavelengths, becomes important in the tropical lower stratosphere, where the atmosphere is very close to radiative equilibrium.

Heating in the stratosphere is assumed to occur as a result of two processes: 1) absorption of the direct beam, which is depleted both by absorption and Rayleigh single scattering, and 2) absorption of diffuse radiation backscattered by the lower atmosphere. The second process is modeled by a pure absorption region on top of a reflecting layer (see Strobel 1978). The effective lower atmosphere albedo is determined as a function of wavelength using the adding method (Lacis and Hansen 1974) and delta-Eddington approximation (Joseph et al. 1976). In the case of water vapor, the integration over wavelength is replaced with the *k*-distribution method of Lacis and Hansen (1974). The probability distribution of water vapor absorption coefficients is taken from Somerville et al. (1974), whereas latitude-dependent ground albedos required for the multiple-scattering computation are from Sellers (1965).

The diurnally averaged solar heating is calculated by the same method as in Cunnold et al. (1975), that is, the heating field is computed for two distinct solar hour angles, the results added, and the sum divided by the empirical constant 2.05. This approximation yields relative errors of about 5%.

The radiative code has been designed to handle several layers of randomly overlapped tropospheric clouds. The treatment of cloudy-sky infrared radiative transfer is simplified by the assumption that negligible cooling takes place below and in between clouds. Allowance is made for nonperfect blackbodies by multiplying the cloud cover of each cloud layer by the input cloud emissivity. The cloud fractions are unchanged for the purpose of calculating the absorption of solar radiation. Cloud visible optical depths are specified for each cloud layer and are used to determine the reflection and transmission functions (averaged over clear and cloudy areas) used in the adding method.

4. Model heating rates

A radiative transfer algorithm must yield accurate and reliable results if it is to be useful in assessing the atmosphere's response to minor perturbations in heating. Since there is no direct measurement of heating rates, accuracy will be judged by comparing model results to those generated by the most rigorous methods (namely, line-by-line radiative calculations). Sensitivity to commonly used input datasets will also be tested.

a. Comparison with LBL results

The effectiveness of the adding method/delta-Eddington approximation relative to other multiple scattering methods has already been discussed by King and Harshvardhan (1986). In this section, we shall compare the heating rates generated by the infrared routines for carbon dioxide, ozone, and water vapor against LBL results reported in the literature. The parameterizations of infrared absorption by methane and nitrous oxide and of near-infrared absorption by water vapor and carbon dioxide, on the other hand, will not be scrutinized in the same manner since these processes individually contribute less than 0.1 K day^{-1} to the heating of the lower stratosphere. As such, these components of the heating, although not negligible, need only be correct to first order.

LBL tropical heating rates for ozone were kindly supplied to us by J. Rosenfield. These were the same heating rates used to validate the IR algorithm of Rosenfield (1991). All other LBL results used here in our comparison were obtained from the GFDL model, courtesy of S. Freidenreich. These include CO_2 heating rates for tropics and midlatitude summer and H_2O and O_3 heating rates for midlatitude summer, corresponding to ICRCCM intercomparison cases 7, 9, 19, and 23 (see Ellingson et al. 1991). (GFDL LBL tropical heating rates for ozone were not available.)

The model atmosphere used to validate the IR code is based on the midlatitude summer and tropical soundings of McClatchey et al. (1971). These soundings were chosen because of their prominence in the ICRCCM (Luther and Fouquart 1984; Ellingson and Fouquart 1991). Model heating rates were calculated using grids identical to those of the LBL calculations.

The largest contributor to the IR cooling rate is carbon dioxide, which makes it more important to have an accurate algorithm for this component of a radiative code. Tables 4 and 5 display the infrared heating due to carbon dioxide as computed with our radiative code versus corresponding rates generated by the GFDL LBL model for tropics and middle-latitude summer. At midlatitude, our results agree with LBL heating rates largely within 5% throughout the stratosphere, with the largest error being 5.8% at two isolated levels. The same is essentially true in the tropics, except near the stratopause, where the error is 10%, and in the tropical lower stratosphere, where, although the absolute errors are

TABLE 4. Carbon dioxide IR heating rates for McClatchey tropical profile.

p (mb)	LBL	Model	Percent difference
0.20011	−3.8267	−4.3136	12.7
0.23332	−4.1147	−4.3391	5.5
0.27203	−4.4283	−4.4507	0.5
0.31716	−4.7851	−4.6601	−2.6
0.36978	−5.1937	−5.0558	−2.7
0.43113	−5.6717	−5.5119	−2.8
0.50266	−6.2490	−6.1638	−1.4
0.58606	−6.9548	−7.0096	0.8
0.68330	−7.6485	−7.5905	−0.8
0.79667	−7.7191	−7.4899	−3.0
0.92885	−7.1439	−7.2688	1.7
1.08300	−6.5775	−7.1468	8.7
1.26260	−6.1717	−6.8404	10.8
1.47210	−5.8407	−6.2483	7.0
1.71640	−5.4124	−5.5100	1.8
2.00110	−4.9013	−4.9088	0.2
2.33320	−4.4391	−4.3721	−1.5
2.72030	−4.0444	−3.9909	−1.3
3.17160	−3.7020	−3.6239	−2.1
3.69780	−3.4003	−3.3581	−1.2
4.31130	−3.1338	−3.0828	−1.6
5.02660	−2.8950	−2.8755	−0.7
5.86060	−2.6781	−2.6485	−1.1
6.83300	−2.4783	−2.4688	−0.4
7.96670	−2.2915	−2.2611	−1.3
9.28850	−2.1144	−2.0979	−0.8
10.8300	−1.9444	−1.8886	−2.9
12.6260	−1.7801	−1.7074	−4.1
14.7210	−1.6211	−1.5633	−3.6
17.1640	−1.4674	−1.4068	−4.1
20.0110	−1.3195	−1.2751	−3.4
23.3320	−1.1793	−1.1207	−5.0
27.2030	−1.0466	−0.9995	−4.5
31.7160	−0.9242	−0.8908	−3.6
36.9780	−0.8160	−0.7975	−2.3
43.1130	−0.7035	−0.6500	−7.6
50.2660	−0.5242	−0.4588	−12.5
58.6060	−0.3352	−0.2954	−11.9
68.3300	−0.1708	−0.1338	−21.6
79.6670	−0.0119	0.0481	−504.5
92.8850	0.1758	0.2007	14.2

always less than 0.07 K day^{-1}, the relative error is high near a zero crossing.

Our model water vapor heating rates, shown in Table 6, have an accuracy of 5% in the lower stratosphere (below 10 mb). The relative error is increasingly larger above 10 mb. We have opted not to implement a more accurate water vapor scheme above 10 mb to account for Doppler broadening in the layer exchange terms because of the high cost in computation time and the fact that water vapor is comparatively unimportant radiatively in this region.

Our middle-latitude summer ozone heating rates, shown in Table 7, agree with LBL calculation to within 5% throughout the stratosphere, except in the vicinity of the zero crossing in the heating rates, where the relative errors are large but the absolute errors are actually very small (less than 0.03 K day^{-1}). The comparison for the tropical atmosphere provides the most stringent test for ozone, since the heating of the equatorial lower stratosphere is an especially delicate balance among competing terms consisting of cooling to space, warming by the surface, and interaction with neighboring atmospheric levels. Rosenfield (1991) found that her original IR scheme produced heating rates for the 9.6-micron band that were in precise agreement (within 5%) with LBL calculations at extratropical latitudes. Within the equatorial lower stratosphere, however, her model overestimated the heating by as much as 0.1 K day^{-1} compared to the LBL results, representing a relative difference of about 16% at around 40 mb. Our results in Table 8 are significantly better below the 20-mb level than those reported in Rosenfield (1991), which demonstrates how sensitive the ozone scheme is to the vertical quadrature and absorption-path scaling

TABLE 5. Carbon dioxide IR heating rates for McClatchey midlatitude summer profile.

p (mb)	LBL	Model	Percent difference
0.20011	−3.3187	−3.8490	16.0
0.23332	−3.6213	−3.9544	9.2
0.27203	−3.9444	−4.0389	2.4
0.31716	−4.3016	−4.2231	−1.8
0.36978	−4.7057	−4.5781	−2.7
0.43113	−5.1651	−4.9763	−3.7
0.50266	−5.6958	−5.5727	−2.2
0.58606	−6.3202	−6.3591	0.6
0.68330	−7.0755	−7.2946	3.1
0.79667	−8.0040	−8.4576	5.7
0.92885	−8.8590	−8.7647	−1.1
1.08300	−8.5988	−8.6923	1.1
1.26260	−7.8594	−8.1613	3.8
1.47210	−7.0868	−7.0767	−0.1
1.71640	−6.3344	−6.1578	−2.8
2.00110	−5.6553	−5.4701	−3.3
2.33320	−5.0656	−4.8589	−4.1
2.72030	−4.5557	−4.3527	−4.5
3.17160	−4.1107	−3.9369	−4.2
3.69780	−3.7179	−3.5703	−4.0
4.31130	−3.3677	−3.2526	−3.4
5.02660	−3.0566	−2.9751	−2.7
5.86060	−2.7958	−2.7770	−0.7
6.83300	−2.5816	−2.5554	−1.0
7.96670	−2.3871	−2.3856	−0.1
9.28850	−2.1984	−2.1793	−0.9
10.8300	−2.0131	−1.9525	−3.0
12.6260	−1.8301	−1.7912	−2.1
14.7210	−1.6484	−1.5959	−3.2
17.1640	−1.4667	−1.4087	−4.0
20.0110	−1.2876	−1.2523	−2.7
23.3320	−1.1305	−1.1142	−1.4
27.2030	−1.0193	−1.0284	0.9
31.7160	−0.9304	−0.9208	−1.0
36.9780	−0.8381	−0.8265	−1.4
43.1130	−0.7395	−0.7272	−1.7
50.2660	−0.6368	−0.6231	−2.2
58.6060	−0.5308	−0.5117	−3.6
68.3300	−0.4205	−0.3962	−5.8
79.6670	−0.3173	−0.3055	−3.7
92.8850	−0.2575	−0.2496	−3.1

TABLE 6. Water vapor IR heating rates for McClatchey midlatitude summer profile.

p (mb)	LBL	Model	Percent difference
0.20011	−0.5442	−1.4455	165.6
0.23332	−0.5848	−1.3986	139.2
0.27203	−0.6292	−1.3420	113.3
0.31716	−0.6787	−1.2899	90.0
0.36978	−0.7348	−1.2538	70.6
0.43113	−0.7981	−1.2132	52.0
0.50266	−0.8704	−1.1911	36.9
0.58606	−0.9541	−1.1799	23.7
0.68330	−1.0531	−1.1738	11.5
0.79667	−1.1683	−1.1708	0.2
0.92885	−1.2634	−1.1404	−9.7
1.08300	−1.2274	−1.0576	−13.8
1.26260	−1.1276	−0.9611	−14.8
1.47210	−1.0226	−0.8594	−16.0
1.71640	−0.9246	−0.7721	−16.5
2.00110	−0.8409	−0.7044	−16.2
2.33320	−0.7727	−0.6454	−16.5
2.72030	−0.7177	−0.5977	−16.7
3.17160	−0.6727	−0.5588	−16.9
3.69780	−0.6347	−0.5264	−17.1
4.31130	−0.6018	−0.4988	−17.1
5.02660	−0.5727	−0.4754	−17.0
5.86060	−0.5486	−0.4593	−16.3
6.83300	−0.5288	−0.4428	−16.3
7.96670	−0.5105	−0.4307	−15.6
9.28850	−0.4923	−0.4347	−11.7
10.83300	−0.4740	−0.4450	−6.1
12.6260	−0.4554	−0.4482	−1.6
14.7210	−0.4363	−0.4306	−1.3
17.1640	−0.4165	−0.4127	−0.9
20.0110	−0.3962	−0.3961	−0.0
23.3320	−0.3781	−0.3828	1.2
27.2030	−0.3657	−0.3726	1.9
31.7160	−0.3561	−0.3636	2.1
36.9780	−0.3458	−0.3539	2.3
43.1130	−0.3341	−0.3428	2.6
50.2660	−0.3210	−0.3301	2.8
58.6060	−0.3066	−0.3157	3.0
68.3300	−0.2904	−0.3011	3.7
79.6670	−0.2746	−0.2891	5.3
92.8850	−0.2661	−0.2803	5.3

method. Note that the larger relative percentage errors between 7 and 20 mb are again in the vicinity of the zero crossing in the heating rates and correspond to absolute differences of no more than 0.05 K day^{-1}. Above the 7-mb level, the majority of the deviations are under 5%, with none over 10%.

In summary, our IR code produces heating rates for individual component in good agreement with LBL calculations, with an accuracy of 5% in relative error or 0.1 K day^{-1} in absolute error in the lower stratosphere. Tables 9 and 10 compare the total IR cooling (including line overlap) for CO_2, H_2O, and O_3 from our radiative code with the total cooling from the GFDL model in the tropics and at midlatitudes, which shows that they agree with each other within 10% throughout much of the stratosphere except, of course, near a zero crossing, with absolute errors less than 0.05 K day^{-1} in the lower stratosphere. It therefore appears that errors in individual IR components do not accumulate in the net IR heating rate.

b. *Effects of input data*

Biases in (satellite) data of temperature and ozone used in radiative calculations have often been cited as a cause for large imbalances found in some published heating rates. This problem is addressed here by using three different sets of input data in our diagnostic calculation of the global heating rates in the stratosphere for the month of January. The first set is comprised of 1979 LIMS data for temperature and ozone between 0.1 and 100 mb. The second set employs the CIRA climatology for the temperature field above 100 mb (Barnett and Corney 1985) and the revised SBUV January 1979 ozone field (Fleig et al. 1990) between 2 and 100 mb. CIRA ozone values (Keating and Young

TABLE 7. Ozone IR heating rates for McClatchey midlatitude summer profile.

p (mb)	LBL	Model	Percent difference
0.20011	−0.1802	−0.2280	26.5
0.23332	−0.2860	−0.3568	24.8
0.27203	−0.4044	−0.4944	22.3
0.31716	−0.5354	−0.6260	16.9
0.36978	−0.6790	−0.7781	14.6
0.43113	−0.8353	−0.9400	12.5
0.50266	−1.0051	−1.1294	12.4
0.58606	−1.1889	−1.3318	12.0
0.68330	−1.3865	−1.5140	9.2
0.79667	−1.5875	−1.6739	5.4
0.92885	−1.7520	−1.7625	0.6
1.08300	−1.9619	−1.9177	−2.3
1.26260	−2.0085	−1.9482	−3.0
1.47210	−1.8988	−1.8121	−4.6
1.71640	−1.7099	−1.6277	−4.8
2.00110	−1.6158	−1.5960	−1.2
2.33320	−1.4855	−1.5148	2.0
2.72030	−1.3227	−1.3653	3.2
3.17160	−1.1602	−1.2085	4.2
3.69780	−0.9978	−1.0370	3.9
4.31130	−0.8513	−0.8691	2.1
5.02660	−0.7264	−0.7358	1.3
5.86060	−0.6222	−0.6335	1.8
6.83300	−0.5357	−0.5360	0.0
7.96670	−0.4572	−0.4434	−3.0
9.28850	−0.3805	−0.3527	−7.3
10.8300	−0.3041	−0.2813	−7.5
12.6260	−0.2273	−0.2105	−7.4
14.7210	−0.1406	−0.1133	−19.4
17.1640	−0.0591	−0.0360	−39.0
20.0110	0.0122	0.0242	98.3
23.3320	0.0715	0.0745	4.3
27.2030	0.1182	0.1179	−0.3
31.7160	0.1569	0.1633	4.1
36.9780	0.1947	0.2013	3.4
43.1130	0.2341	0.2345	0.2
50.2660	0.2650	0.2617	−1.3
58.6060	0.2818	0.2766	−1.8
68.3300	0.2918	0.2863	−1.9
79.6670	0.2816	0.2763	−1.9
92.8850	0.2567	0.2521	−1.8

TABLE 8. Ozone IR heating rates for McClatchey tropical profile.

p (mb)	LBL	Model	Percent difference
0.12173	−0.0466	−0.0429	−7.9
0.16632	−0.2117	−0.1983	−6.3
0.22725	−0.4360	−0.4188	−3.9
0.31051	−0.7253	−0.7236	−0.2
0.42426	−1.0534	−1.0443	−0.9
0.57970	−1.3942	−1.3518	−3.0
0.79207	−1.6669	−1.5869	−4.8
1.08230	−1.7846	−1.6915	−5.2
1.47870	−1.7106	−1.6412	−4.1
2.02050	−1.4790	−1.4832	0.3
2.76070	−1.1471	−1.2250	6.8
3.77210	−0.8087	−0.8776	8.5
5.15400	−0.5496	−0.5879	7.0
7.04220	−0.3685	−0.4079	10.7
9.62220	−0.1870	−0.2244	20.0
13.1470	0.0556	0.0188	−66.1
17.9640	0.2969	0.2511	−15.4
24.5450	0.4719	0.4263	−9.7
33.5370	0.5774	0.5590	−3.2
45.8240	0.5660	0.5703	0.8
62.6120	0.4367	0.4360	−0.2
85.5500	0.2231	0.2163	−3.1

1985) are used above 2 mb and whenever SBUV data are unavailable between 2 and 100 mb. Because the global coverage of the LIMS data is limited to latitudes between 64°S and 84°N, we use ozone mixing ratios and temperatures from the second dataset to fill in the first at latitudes poleward of 64°S. The third set differs from the second only in that NMC temperatures for 1 January 1979 are used between 1 and 100 mb. These three sets of input data will be referred to as LIMS, CIRA, and NMC input.

All three sets of data make use of LIMS values of water vapor and nitrogen dioxide mixing ratio above 100 mb and 1979 SAMS observations of methane and nitrous oxide. Missing values near the pole for any of these absorbers are set equal to the corresponding mixing ratio at the first equatorward grid for which data is reported. Values for the mixing ratios of water vapor and nitrogen dioxide above the altitude range of the LIMS measurements are filled in by assuming that they decrease exponentially with height. Methane and nitrous oxide mixing ratios, on the other hand, are set equal to 50 ppbv and 0.1 ppbv, respectively, when not reported by SAMS in the upper stratosphere and mesosphere.

The tropospheric climatology required employs NMC temperatures for 1 January 1979 and water vapor mixing ratios computed from the surface temperature-dependent relative humidity parameterization of Cess (1976). Ozone values in the troposphere are filled in according to the following empirical formula from Green (1964):

$$C(z) = \frac{\alpha[1 + \exp(-\beta/\gamma)]}{1 + \exp[(z - \beta)/\gamma]}, \qquad (41)$$

where $C(z)$ is the ozone column (cm, NTP) above an altitude z, α the total column above the surface, β the altitude of the maximum ozone concentration, and $\alpha[1 + \exp(-\beta/\gamma)]/(4\gamma)$ the maximum ozone concentration. Total ozone columns used in Eq. (41) are specified from Keating and Young (1985), whereas methane and nitrous oxide mixing ratios are set to 1.6 and 0.3 ppmv, respectively, below the altitude range of the SAMS measurements.

The two-dimensional grid employed for the diagnostic calculation has 18 equally spaced latitudes from 85°S to 85°N and 63 pressure levels from the surface to 0.1 mb. This corresponds to a vertical resolution of approximately 1 km in the stratosphere and mesosphere. Below 100 mb, the grid levels are separated by a pressure difference of 50 mb. A uniform mixing ratio of 330 ppmv is assumed for carbon dioxide, as is ap-

TABLE 9. Total IR heating rates for McClatchey tropical profile.

p (mb)	LBL	Model	Percent difference
0.2001	−4.8074	−6.1050	27.0
0.2333	−5.2594	−6.2111	18.1
0.2720	−5.7533	−6.4245	11.7
0.3172	−6.3086	−6.7407	6.8
0.3698	−6.9347	−7.2839	5.0
0.4311	−7.6514	−7.8801	3.0
0.5027	−8.4912	−8.6767	2.2
0.5861	−9.4775	−9.6638	2.0
0.6833	−10.4120	−10.3150	−0.9
0.7967	−10.5320	−10.1500	−3.6
0.9288	−9.9652	−9.8804	−0.9
1.0830	−9.4212	−9.7196	3.2
1.2626	−8.9639	−9.3007	3.8
1.4721	−8.5216	−8.5544	0.4
1.7164	−8.0047	−7.6757	−4.1
2.0011	−7.3825	−6.9467	−5.9
2.3332	−6.7399	−6.2419	−7.4
2.7203	−6.1508	−5.6879	−7.5
3.1716	−5.6125	−5.1465	−8.3
3.6978	−5.1134	−4.7091	−7.9
4.3113	−4.6694	−4.2745	−8.5
5.0266	−4.2677	−3.9250	−8.0
5.8606	−3.8994	−3.5653	−8.6
6.8330	−3.5803	−3.2806	−8.4
7.9667	−3.2683	−2.9614	−9.4
9.2885	−2.9506	−2.7134	−8.0
10.8300	−2.6264	−2.4161	−8.0
12.6260	−2.2914	−2.1098	−7.9
14.7210	−1.9606	−1.8474	−5.8
17.1640	−1.6543	−1.5965	−3.5
20.0110	−1.3663	−1.3584	−0.6
23.3320	−1.0899	−1.0819	−0.7
27.2030	−0.8326	−0.8529	2.4
31.7160	−0.6270	−0.6792	8.3
36.9780	−0.4808	−0.5444	13.2
43.1130	−0.3652	−0.3703	1.4
50.2660	−0.1932	−0.1714	−11.3
58.6060	−0.0527	−0.0454	−13.9
68.3300	0.0327	0.0547	67.5
79.6670	0.1104	0.1813	64.3
92.8850	0.2429	0.2507	3.2

TABLE 10. Total IR heating rates for McClatchey midlatitude summer profile.

p (mb)	LBL	Model	Percent difference
0.2001	−4.1191	−5.5231	34.1
0.2333	−4.5839	−5.7106	24.6
0.2720	−5.0869	−5.8762	15.5
0.3172	−5.6434	−6.1398	8.8
0.3698	−6.2676	−6.6109	5.5
0.4311	−6.9685	−7.1305	2.3
0.5027	−7.7645	−7.8942	1.7
0.5861	−8.6815	−8.8718	2.2
0.6833	−9.7599	−9.9834	2.3
0.7967	−11.0310	−11.3030	2.5
0.9288	−12.1700	−11.6690	−4.1
1.0830	−12.1280	−11.6690	−3.8
1.2626	−11.3680	−11.0720	−2.6
1.4721	−10.3930	−9.7499	−6.2
1.7164	−9.3539	−8.5596	−8.5
2.0011	−8.5195	−7.7729	−8.8
2.3332	−7.7440	−7.0219	−9.3
2.7203	−7.0122	−6.3190	−9.9
3.1716	−6.3436	−5.7078	−10.0
3.6978	−5.7211	−5.1377	−10.2
4.3113	−5.1567	−4.6248	−10.3
5.0266	−4.6563	−4.1910	−10.0
5.8606	−4.2330	−3.8750	−8.5
6.8330	−3.8803	−3.5398	−8.8
7.9667	−3.5584	−3.2659	−8.2
9.2885	−3.2450	−2.9735	−8.4
10.8300	−2.9358	−2.6865	−8.5
12.6260	−2.6291	−2.4583	−6.5
14.7210	−2.3085	−2.1486	−6.9
17.1640	−1.9953	−1.8665	−6.5
20.0110	−1.7003	−1.6338	−3.9
23.3320	−1.4472	−1.4326	−1.0
27.2030	−1.2635	−1.2942	2.4
31.7160	−1.1163	−1.1329	1.5
36.9780	−0.9685	−0.9917	2.4
43.1130	−0.8136	−0.8490	4.4
50.2660	−0.6647	−0.7059	6.2
58.6060	−0.5277	−0.5656	7.2
68.3300	−0.3938	−0.4260	8.2
79.6670	−0.2893	−0.3332	15.2
92.8850	−0.2511	−0.2917	16.2

propriate for the period of the LIMS observations. Three layers of tropospheric clouds are specified according to climatological data (Newell et al. 1974). Input cloud emissivities are 0.3 for high clouds and unity for middle and low clouds. Cloud visible optical depths, on the other hand, are set at 2, 8, and 16 for high, middle, and low clouds, respectively.

The model total heating rates for the above specified inputs are shown in Fig. 2. These results may be compared with those reported in the studies of Kiehl and Solomon (1986) and Rosenfield et al. (1987) for the month of January. We especially note two differences present in our results regardless of the inputs. First, our maximum net heating rates in the summer upper stratosphere are less by a factor of 2 than those of Rosenfield et al. (1987) but are in closer agreement with the diabatic heating rates of Kiehl and Solomon (1986) in the same vicinity. Second, our positive heating rates obtained in the tropical lower stratosphere are substantially lower than in either of the aforementioned studies. Note, for example, that at 30 km near the tropics, the net diabatic heating from both Kiehl and Sol-

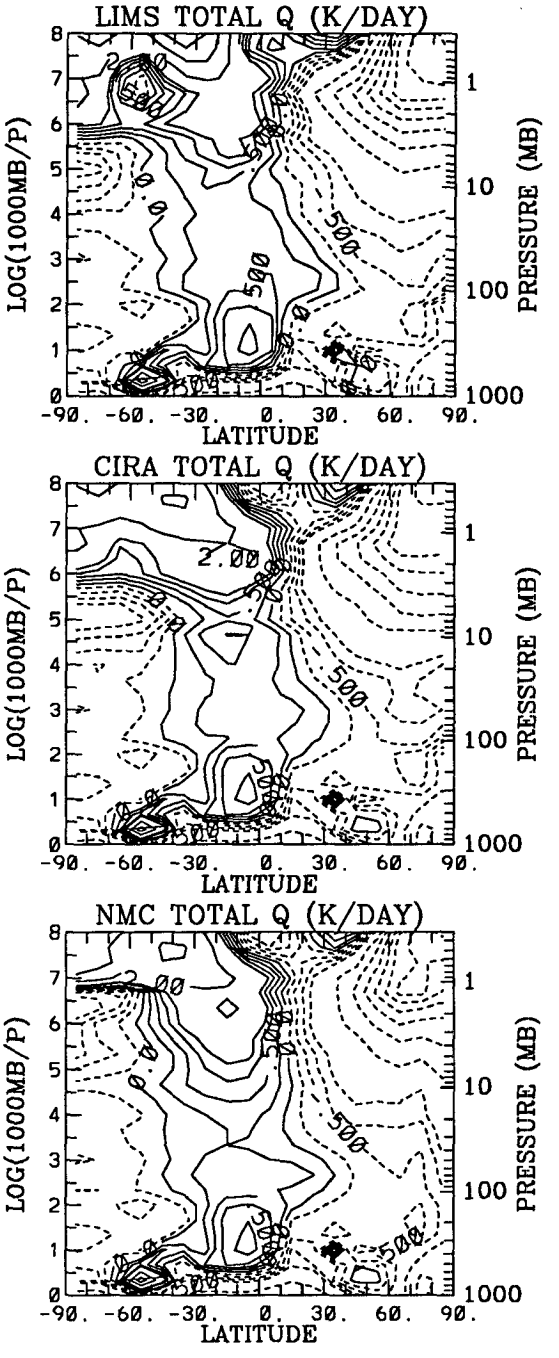

FIG. 2. Model produced net heating rates using three input datasets: (a) LIMS; (b) CIRA; (c) NMC. Contour values are ±0.25, 0.5, 0.75, 1.0, 2.0, 3.0, ...

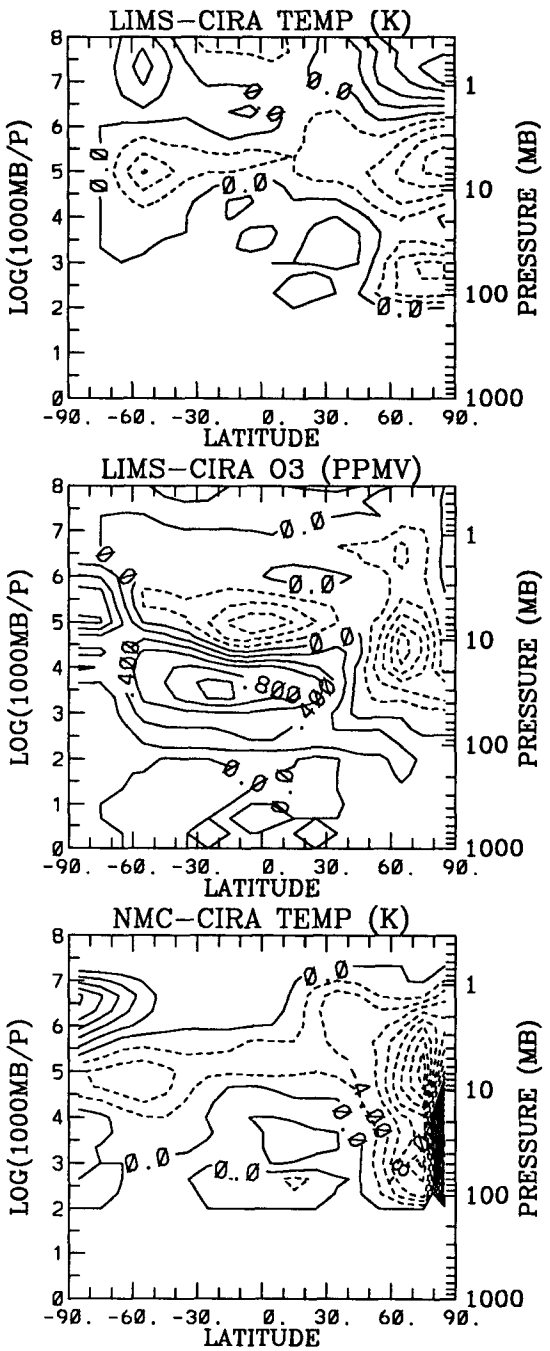

FIG. 3. The differences between inputs used to produce Fig. 2: (a) temperature difference between LIMS and CIRA; (b) Ozone mixing ratio difference between LIMS and CIRA; (c) temperature difference between LIMS and NMC. Contour intervals are 2 K for temperatures and 0.2 ppmv for ozone mixing ratio.

omon (1986) and Rosenfield et al. (1987) is about 1 K day^{-1}, while ours is about 0.5 K day^{-1} or less. Our net heating rate in the tropical lower stratosphere is of the order of +0.3 K day^{-1}. Theirs are presumably higher, but this is difficult to tell from the published figures.

In Fig. 3 we show the differences between the input fields, while the differences between the heating rates are shown in Fig. 4. NMC temperature differs from the CIRA climatology by about ±2°–4° in much of the stratosphere (see Fig. 3c); near northern high latitudes during the polar night the temperatures show large differences. Similar patterns between Figs. 3c and 4b show that warmer (cooler) temperatures produce more (less) IR cooling, thus more negative (positive) total heating rates, as expected. Every 1-K change in temperature produces a heating rate change of about 0.2 K day^{-1} in the upper stratosphere and 0.07 K day^{-1} in the lower stratosphere, giving a radiative relaxation time of about 5 days in the upper stratosphere and 2 weeks in the lower stratosphere.

The difference in net heating rates between LIMS and CIRA inputs include the effects of both temperature and ozone field differences. Note that Fig. 3a shows a region of negative temperature difference between 30°N and 40°S above the 1-mb level, whereas Fig. 3b shows positive ozone differences at nearly all latitudes

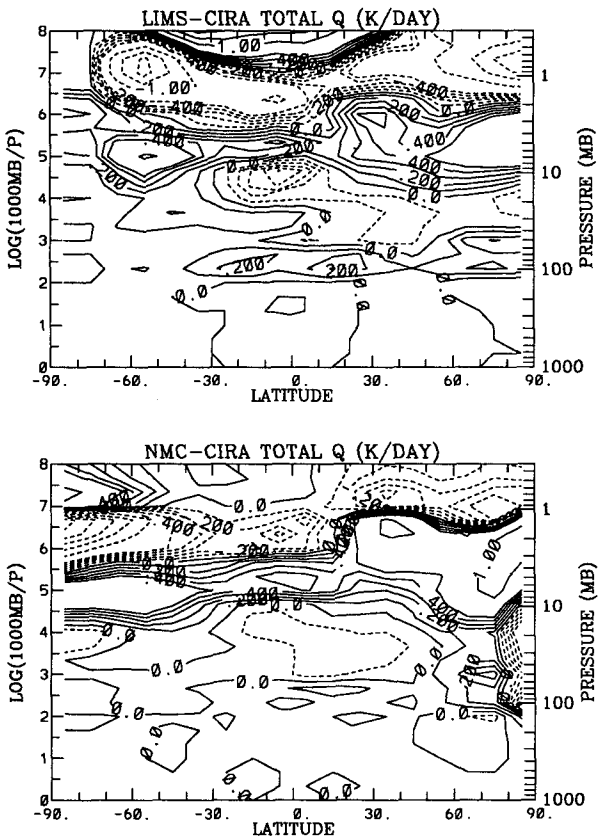

FIG. 4. Model calculated net heating rate differences: (a) LIMS − CIRA; (b) NMC − CIRA. Contour values are ±0.1, 0.2, 0.3, 0.4, 0.5, 1.0, 1.5, 2.0, ... See text for case definitions.

at the same heights. It is known that LIMS temperatures above 1 mb are generally lower than rocketsonde measurements seem to indicate (Gille et al. 1984), and therefore ozone mixing ratios in the mesosphere as deduced from LIMS may be higher than the true values because of the retrieval process linking ozone to the temperature field. The correction of both these errors would result in decreased solar heating together with increased IR cooling, as shown in Fig. 4a.

Figure 4a shows heating rate differences of LIMS–CIRA in the summer upper stratosphere of about -1 K day^{-1}. The results reported by Kiehl and Solomon (1986), which were also based on LIMS data, should resemble the heating rates of Fig. 2a if their algorithm is accurate as judged by comparison with line-by-line infrared codes. However, their heating rates for the upper stratosphere are more similar to those presented in Fig. 2b, which were obtained using CIRA input. Their algorithm apparently underestimates the infrared cooling of the upper stratosphere, which may be due to their simple treatment of Doppler broadening in addition to the inherent shortcomings of the Malkmus model at pressures below 1 mb (see section 3a).

A comparison of LIMS ozone values with balloon measurements indicates that the LIMS instrument also overestimates ozone in the lower stratosphere. Figure 3b shows positive ozone differences that reach about 1 ppmv in this region. Moreover, the new SBUV mixing ratios are almost half as much as the corresponding LIMS values in the tropics near 100 mb. The greater lower stratospheric ozone mixing ratios in LIMS input increase the local heating by both infrared exchange with the surface and absorption of visible solar radiation, leading to a more positive heating rate between 70 and 100 mb, as shown in Fig. 4a.

In summary, the total heating rates change by about 0.1 K day^{-1} in the lower stratosphere and by as much as 1 K day^{-1} in the upper stratosphere due to the different input data used here. Surprisingly, however, the globally integrated heating and cooling are in marginally acceptable balance throughout the stratosphere for all three input sets (see Tables 11 and 12). Therefore, it can be tentatively concluded that the differences in these temperature and ozone datasets are not the cause of large imbalances found in some previously reported radiative calculations.

5. Intercomparison of the effect of different approximations

In this section, we shall compare the net radiative heating rates produced by various methods currently in use in 2D modeling, and try to reproduce and explain some of the heating rate differences among the models. For this purpose, our model with CIRA climatology input used as the basis of comparison will be called the standard (STAN) case.

a. IR parameterization

We consider two cases of different IR parameterization methods called BBCD and BBOZ. BBCD differs from the standard case in that broadband emissivity parameterizations are used exclusively for the CO_2 and H_2O IR computations. That is, the cooling-to-space terms for carbon dioxide and water vapor are computed in the same manner as the layer-exchange terms. BBOZ differs from the standard case in that the ozone IR broadband parameterization of Rodgers (1968) is used in place of the more accurate scheme based on Rosen-

TABLE 11. Model-weighted horizontal (isentropic) averaged net radiative heating rate $\bar{Q}$ (K day^{-1}).

θ (K)	LIMS	CIRA	NMC	BBCD	BBOZ	CLSK	UNAL	LOWR	COMB
2466	0.81	0.27	0.25	0.71	0.39	0.24	0.27	0.79	0.90
2242	0.22	0.36	0.35	1.07	0.50	0.31	0.35	0.83	0.96
2038	−0.31	0.22	0.01	1.20	0.32	0.15	0.21	0.73	0.81
1853	−0.71	−0.09	−0.34	1.25	−0.08	−0.18	−0.11	0.45	0.44
1685	−0.81	−0.32	−0.36	0.91	−0.41	−0.41	−0.33	0.06	−0.05
1532	−0.41	−0.19	−0.18	0.58	−0.37	−0.29	−0.18	−0.02	−0.22
1392	−0.37	−0.38	−0.22	0.12	−0.60	−0.48	−0.35	−0.19	−0.44
1266	−0.43	−0.58	−0.24	−0.20	−0.79	−0.68	−0.52	−0.35	−0.59
1151	−0.37	−0.70	−0.24	−0.38	−0.86	−0.80	−0.63	−0.48	−0.67
1046	−0.26	−0.66	−0.14	−0.41	−0.76	−0.75	−0.56	−0.43	−0.56
951	−0.31	−0.56	−0.15	−0.38	−0.61	−0.64	−0.45	−0.32	−0.40
865	−0.24	−0.30	−0.10	−0.09	−0.29	−0.37	−0.19	−0.08	−0.10
786	−0.22	−0.21	−0.16	−0.04	−0.16	−0.27	−0.11	−0.03	0.00
715	−0.18	−0.16	−0.18	0.07	−0.08	−0.20	−0.06	−0.01	0.06
650	−0.12	−0.13	−0.19	0.04	−0.04	−0.16	−0.05	−0.01	0.09
591	−0.05	−0.10	−0.15	0.02	0.00	−0.10	−0.02	0.01	0.11
537	−0.06	−0.07	−0.12	0.00	0.02	−0.06	0.00	0.01	0.10
488	−0.01	−0.03	−0.04	−0.02	0.04	−0.01	0.02	0.03	0.11
444	0.04	−0.05	−0.01	−0.09	−0.01	−0.03	−0.01	0.02	0.06
404	0.02	−0.09	−0.07	−0.15	−0.08	−0.08	−0.07	0.00	0.02
367	0.13	0.07	0.07	0.06	0.06	0.07	0.07	0.09	0.09

TABLE 12. Horizontal (isobaric) averaged net radiative heating rate $\langle Q \rangle_p$ (K day^{-1}).

p (mb)	LIMS	CIRA	NMC	BBCD	BBOZ	CLSK	UNAL	LORE	COMB
0.2	0.77	−0.74	−0.77	−0.78	−0.71	−0.73	−0.71	−0.33	−0.30
0.3	1.34	0.25	0.22	0.45	0.34	0.25	0.28	0.84	0.93
0.4	0.66	0.24	0.19	0.62	0.36	0.21	0.24	0.79	0.90
0.5	0.30	0.16	0.10	0.71	0.30	0.11	0.15	0.65	0.79
0.7	−0.34	0.19	0.12	0.93	0.32	0.13	0.17	0.78	0.91
1.0	−0.73	−0.05	−0.23	1.22	0.01	−0.12	−0.06	0.65	0.70
1.5	−1.27	−0.63	−0.35	0.59	−0.71	−0.72	−0.64	−0.26	−0.36
2.0	−0.44	−0.23	−0.20	0.56	−0.40	−0.32	−0.22	0.03	−0.16
3.0	−0.43	−0.55	−0.25	−0.16	−0.78	−0.65	−0.50	−0.28	−0.55
4.0	−0.48	−0.66	−0.30	−0.33	−0.85	−0.76	−0.59	−0.46	−0.67
5.0	−0.23	−0.66	−0.18	−0.34	−0.79	−0.75	−0.57	−0.45	−0.61
7.0	−0.29	−0.70	−0.16	−0.53	−0.77	−0.79	−0.60	−0.46	−0.56
10.0	−0.21	−0.18	−0.04	0.05	−0.17	−0.26	−0.07	−0.01	−0.02
15.0	−0.19	−0.16	−0.17	0.07	−0.10	−0.22	−0.06	−0.01	0.04
20.0	−0.15	−0.09	−0.19	0.13	0.00	−0.12	0.01	0.04	0.13
30.0	0.01	−0.10	−0.13	0.01	0.01	−0.10	−0.02	0.02	0.13
40.0	−0.01	−0.01	−0.06	0.06	0.09	0.00	0.06	0.07	0.17
50.0	−0.01	0.01	−0.01	0.03	0.08	0.02	0.06	0.08	0.16
70.0	0.15	0.02	0.09	−0.02	0.05	0.04	0.06	0.09	0.12

field (1991). The heating rate differences between these and the standard case are shown in Fig. 5.

The main feature of case BBCD is an underestimate of IR cooling ranging from 0.1 to 0.2 K day^{-1} in the lower stratosphere to as much as 1–3 K day^{-1} near the stratopause (see Fig. 5a). This will lead to a large positive imbalance in horizontally averaged heating near 1 mb, which is present in the study of Callis et al. (1987), who also used the emissivity scheme of Ou and Liou (1983) and temperatures from Barnett and Corney (1985). Crisp et al. (1986) showed that a careful treatment of the transition from pressure to Doppler broadening is essential for an accurate simulation of CO_2 infrared cooling near the stratopause. Rosenfield et al. (1987), like Callis et al. (1987), computed a large positive imbalance near 1 mb. Although their carbon dioxide infrared parameterization implicitly took into account Voigt line shape, it was based on the LBL results of Chou and Kouvaris (1986), which differ from the GFDL results by about 20% owing to a different treatment of the far wings of the CO_2 lines.

The heating rates produced by the ozone IR broadband parameterization of Rodgers (1968) are more positive in the lower stratosphere and are more negative in the upper stratosphere than those produced by the more accurate scheme based on Rosenfield (1991) by about 0.1–0.2 K day^{-1} (see Fig. 5b).

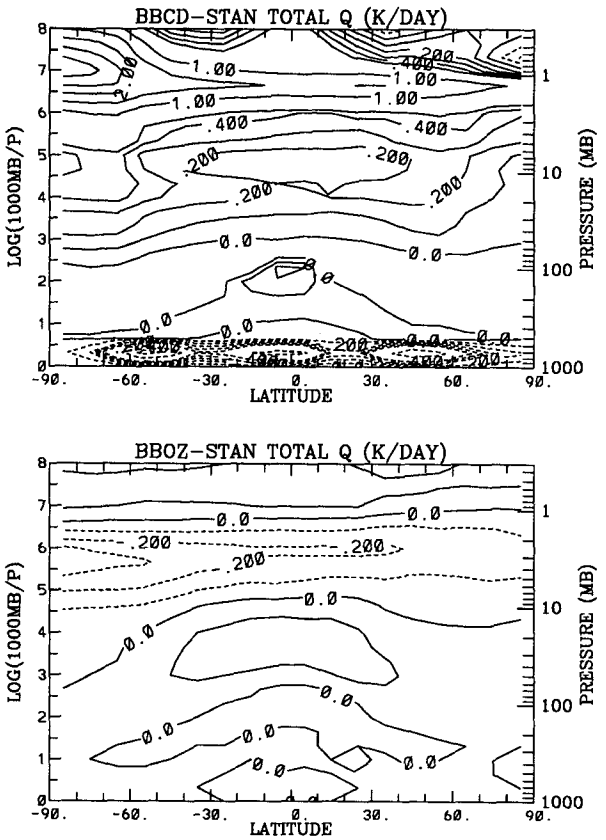

FIG. 5. As in Fig. 4 except for (a) BBCD − STAN; (b) BBOZ − STAN.

b. *Treatment of clouds*

Treatment of the radiative effects of clouds in some (2D) models is often problematic, as we shall illustrate with the following two case runs. The first differs from the standard case by the assumption of clear-sky conditions for both the infrared and solar radiation computations, while the second treats clouds inconsistently. In the second experiment, the effect of the clouds on the infrared radiative balance is ignored, but a uniform albedo for the lower atmosphere is assumed, as was

sometimes done in the literature (e.g., Haigh 1984). These cases will be referred to as CLSK and UNAL, respectively. The resulting heating rates CLSK and UNAL (with an albedo of 0.3) are shown in Fig. 6.

Figure 6a shows that ignoring cloudiness in a consistent fashion has a minimal effect on the diabatic heating of the stratosphere, although large differences exist for the troposphere (which is not the scope of the present study). The effective radiating temperature of the troposphere is lowered in the presence of clouds, resulting in an increase in infrared cooling of the stratosphere, but there is a simultaneous compensating increase in the effective visible albedo of the lower atmosphere, which in turn increases the solar heating at higher levels.

Figure 6b shows that treating clouds inconsistently leads to increased heating in the stratosphere at low and middle latitudes and increased cooling at high latitudes. Such a pattern in heating rate difference will increase the meridional transport from tropics to polar regions and thus has a larger effect on the dynamics of the stratosphere than the horizontally uniform pattern, as shown in Fig. 6a. By assuming a visible albedo of 0.3 for the troposphere, one has effectively "painted" clouds on the surface, particularly near the tropics, where surface albedos are otherwise much lower. The resulting increase in radiation backscattered into the stratosphere is not compensated by any decrease in infrared heating due to the screening of the hot surface by the clouds.

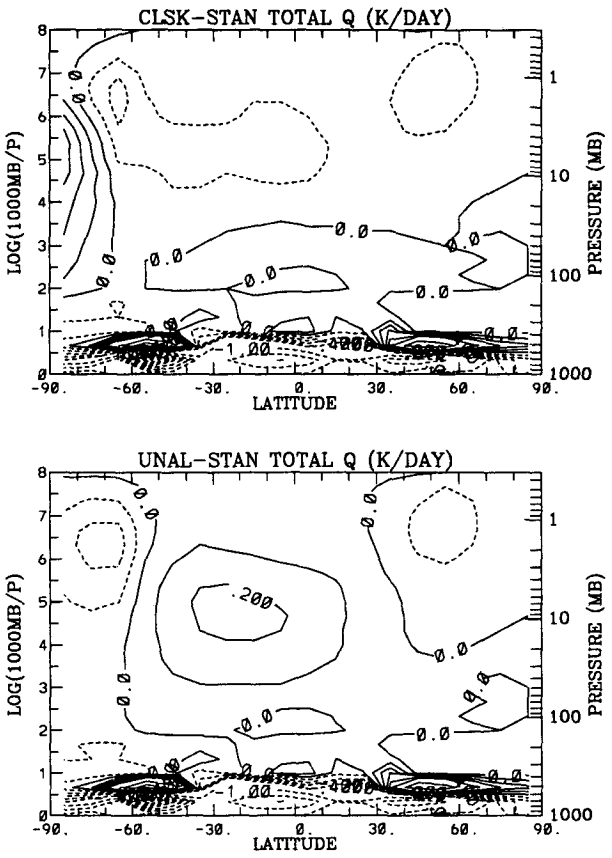

FIG. 6. As in Fig. 4 except for (a) CLSK − STAN; (b) UNAL − STAN.

c. *Effect of numerical treatments*

The vertical resolution adopted in all the aforementioned cases is generally 1 km. However, in practice when a 2D model using the radiative code is used in a long-term simulation, we often find it necessary to use a 2-km vertical resolution (see Yang et al. 1991). When a comparison test of our code was first performed using 1- and 2-km resolutions, relatively large differences were found near the tropical tropopause and in the lower stratosphere just above it. The differences were found to be caused by the sensitivity of the vertical quadrature scheme to the large pressure and temperature differences across layers. The problem can be largely overcome by adopting analytical methods in performing the vertical derivatives and quadratures and by more carefully performing the remaining finite differences.

In our current version of the code, 2-km resolution is tolerably accurate. In our next case run denoted by LORE, we repeat the CIRA experiment with 2-km resolution, and the heating rate difference from the standard case is shown in Fig. 7a. The difference is 0.01 K day^{-1} or less in the lower stratosphere and on the order of 0.2–0.5 K day^{-1} in the upper stratosphere.

However, the accuracy degrades significantly when coarse resolution is coupled with a less accurate infrared scheme. To demonstrate this, another case run is performed, which we label COMB, where half the vertical resolution (as compared to the standard case) is used in combination with the less accurate parameterization of Rosenfield et al. (1987) for the ozone 9.6-micron band [as opposed to the more accurate scheme of Rosenfield (1991)]. The results are shown in Fig. 7b.

In contrast to Fig. 7a, Fig. 7b shows serious errors of +0.2 K day^{-1} in the tropical lower stratosphere. That is, the COMB case has a local net positive heating rate twice as large as the standard case in the equatorial lower stratosphere, with important impact on the transport of chemical tracers in the stratosphere. This type of error is probably common in most 2D models adopting a less accurate broadband parameterization for ozone absorption in combination with a 2-km resolution.

Table 12 indicates that the COMB case has an isobaric imbalance on the order of +0.2 K day^{-1} in the lower stratosphere. This may explain why some previous studies derive imbalance in the lower stratosphere in the same range of +0.2 K day^{-1}. The positive im-

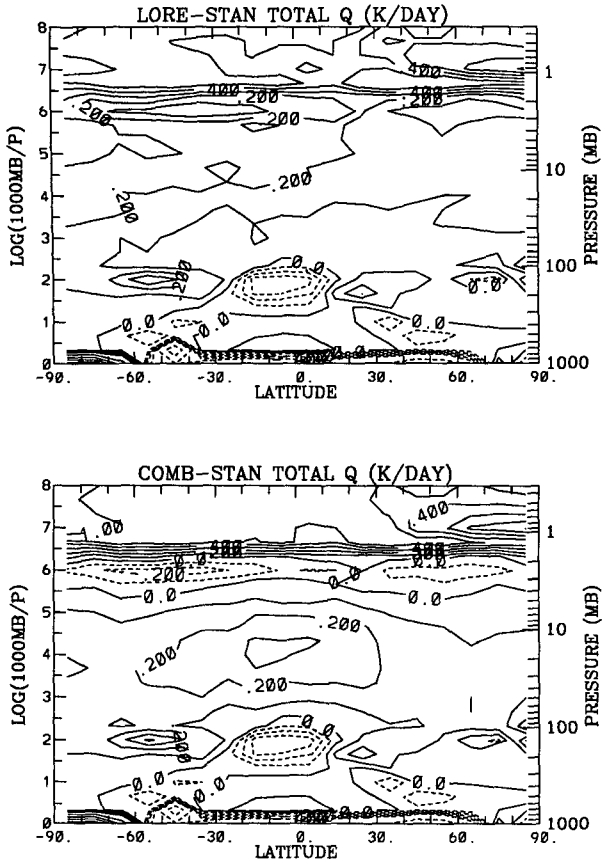

FIG. 7. As in Fig. 4 except for (a) LORE − STAN; (b) COMB − STAN.

balances of Callis et al. (1987) and Rosenfield et al. (1987) are most likely due to their use of inaccurate broadband parameterizations for ozone absorption. Kiehl and Soloman (1986), on the other hand, compute a negative imbalance throughout the stratosphere. Their Fig. 7 indicates a globally averaged excess of infrared cooling over solar heating of about 0.2 K day^{-1} between 20 and 25 km above the surface. Kiehl and Soloman (1986) used a narrowband Malkmus model that should give infrared cooling rates in close agreement with LBL results below 1 mb. We suspect, however, that their implementation of the simple adjustment technique proposed by Fels (1979) to account for Voigt line shape may have overestimated the infrared cooling in the lower stratosphere.

6. Effect on transport

The results of the preceding section are especially significant when applied to the problem of tracer advection in the stratosphere. Some models that account for both transport and photochemistry deduce the effects of large-scale dynamics from precalculated heating rates, while others include a full-scale radiative calculation as part of the numerical simulation. In either case, it is important to understand the effects of errors in the radiative algorithm that generates the heating rates on the advecting field.

If the local heating rates are applied directly to deduce the vertical advection velocity, and if the latitude of interest is in the tropics, then the commonly adopted, less accurate radiative transfer scheme will most likely lead to an overestimate of the equatorial upwelling velocity above the tropopause. In the case of ozone, the increase in mixing ratio with height in the lower stratosphere implies that the vertically integrated ozone column amount will be underestimated as a result of errors in the vertical advection in the tropics, while the ozone column amount will be overestimated in the polar region due to too strong a poleward transport.

In most two-dimensional models, the diabatic heating rates are usually adjusted in order to enforce mass conservation in the resulting transport circulation. However, there is no unique method for doing this, and therefore the adjustment must necessarily be ad hoc. The simplest and most commonly employed method is to subtract the horizontal average heating rate from the local net heating. If there is a negative imbalance in the computed globally averaged heating of the lower stratosphere, such as in the work of Kiehl and Solomon (1986), this method of adjustment will lead to an aggravation of the tropical errors noted previously. If there is a positive imbalance, such as in the work of Rosenfield et al. (1987), the method will have a compensating effect at equatorial latitudes. However, this will be done at the expense of intensifying the downward motion in the poleward branch of the Brewer–Dobson circulation.

The sensitivity of global tracers to small changes in the radiative heating will be illustrated by examining the behavior of ozone in the lower stratosphere within a previously documented two-dimensional model in isentropic coordinates. That model was described in Yang et al. (1991) and includes the radiative transfer algorithm discussed here. However, in order to examine the direct effects of diabatic heating errors on transport rather than those mitigated by complex radiative–dynamical–chemical feedbacks, the model will be run off-line using the heating rates externally calculated for the various cases of section 4. We shall also suppress the annual solar cycle and assume perpetual January conditions. Isentropic diffusion coefficient K_{yy} is calculated consistently with the heating rate of each case (see Yang et al. 1990, 1991).

Figure 8a shows a total ozone column between 10 and 100 mb generated by our 2D model in isentropic coordinates using the net heating field of the standard (CIRA input) case after adjusting for mass conservation by uniformly subtracting the imbalance. [The layer,

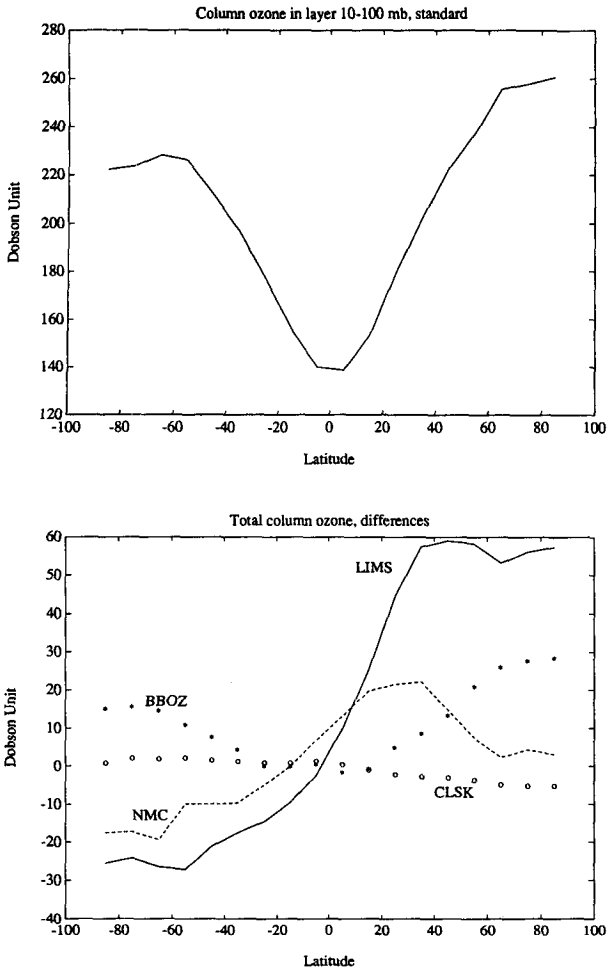

FIG. 8. Model calculated column ozone in layer 10–100 mb: (a) STAN; (b) differences between various cases and STAN.

10–100 mb, is known to be sensitive to dynamical transport, see Yang et al. (1991).] Figure 8b, on the other hand, shows the differences in this predicted quantity between the standard case and other selected cases. As expected the clear-sky case produces ozone distribution virtually identical to that of the standard case in this layer. Here we emphasize relative changes between the various cases to illustrate the sensitivity of transported ozone to changes in heating rate in lower stratosphere. The perpetual January condition used here makes it inappropriate to compare with observational data, although our model result is quite close compared with observations. For model simulation of ozone and other species with full annual cycle, see Yang et al. (1991).

Note that LIMS case produces ozone columns significantly different from the CIRA case at nearly all latitudes. Figure 4a shows a difference of 0.1 K day^{-1} (0.2 K day^{-1} in more limited regions) in heating rates between the two cases in this layer (this is still true after a small heating rate adjustment is made for mass conservation). Compared to the CIRA case, the heating rate for the LIMS case in this layer is generally more negative in the Northern Hemisphere; therefore, the transport to northern high latitudes is stronger, producing more ozone in northern high latitudes. In the Southern Hemisphere, the heating rate for LIMS case in this layer is generally more positive; therefore, the transport to southern high latitudes is weaker, producing less ozone in southern high latitudes. The net effect is a differential transport from the Southern Hemisphere to the Northern Hemisphere. The difference at high latitudes is about 30 to 50 Dobson units or 15%–20% in the layer (see Fig. 8), which clearly demonstrates the kind of sensitivity of transported ozone to changes of heating rate on the order of 0.1–0.2 K day^{-1}. The NMC case produced a similar effect on ozone transport, although the magnitude is smaller.

In contrast, the case of degraded O_3 IR parameterization produced a stronger upwelling in the tropics. Transports to both hemispheres are increased. The ozone column in the layer at high latitudes is about 15–30 DU, or about 10%, higher than the standard case.

The result of Fig. 8 shows clearly that changes on the order of 0.1–0.2 K day^{-1} in the net diabatic heating of the lower stratosphere are sufficient to cause significant changes in the global distribution of ozone and, presumably, in other chemical tracers of relevance to terrestrial climate. Guthrie et al. (1990) in fact showed that using different temperature data as inputs to the radiative transfer code of Rosenfield et al. (1987) produced residual circulations that led to significant differences in the transport of nitrous oxide, particularly in the tropical lower stratosphere. This puts a severe constraint on the accuracy requirement for radiative transfer algorithms used in predictive models of the stratosphere. Moreover, it calls attention to the need for a more careful analysis of the observational inputs required for a proper evaluation of the atmospheric radiative budget.

7. Conclusion

It is known that the global distribution of stratospheric tracers depends critically on the strength of the so-called "Brewer–Dobson" circulation, which consists of generally rising motion in the tropical lower stratosphere and sinking motion over high latitudes in both hemispheres. In fact, the circulation was first inferred by Brewer (1949) and Dobson (1956) from observed distributions of water vapor and ozone. It can also be deduced from direct radiative transfer calculations (Murgatroyd and Singleton 1961; Wehrbein and Leovy 1982; Kiehl and Solomon 1986; Callis et al. 1987; Gille et al. 1987; Rosenfield et al. 1987), which yield a dia-

batic circulation that has theoretically been shown to be mainly responsible for the advective transport of global tracers (Dunkerton 1978; Tung 1982; WMO 1986).

While there is a general consensus on the pattern of the Brewer–Dobson circulation, there is no agreement as to its strength. Of special importance to stratospheric tracers is the magnitude of the upwelling in the tropical lower stratosphere. Shia et al. (1989) found that up to a factor of 3 difference exists among various published diabatic circulation strengths and that carbon-14 data appear to favor a weaker circulation than was previously surmised. Yang et al. (1991) also showed on the basis of model simulations of several stratospheric tracers, including NO_y and O_3, that a weaker circulation is probably appropriate.

Due to various uncertainties in both input data and methods and the fact that the lower stratosphere is close to radiative equilibrium, it is difficult to implement a radiative transfer algorithm that produces errors substantially lower than the actual net radiative heating rates in the region. Compounding the problem is the common occurrence of imbalances in the computed globally averaged net heating that are of the same order of magnitude as the local net heating rates themselves. To ensure mass conservation in transport models, such imbalances are usually subtracted away from the local net heating in an ad hoc fashion, resulting in uncertainties of the order of ±100%.

Theoretically, infrared cooling and solar heating rates should be in balance to within 0.03 K day^{-1} in the lower stratosphere over monthly means. We are currently unable to attain such an accuracy in our radiative calculations. However, it is found that since tracers are sensitive to diabatic circulation differences of over 0.1–0.2 K day^{-1} in the lower stratosphere, the computed heating rates should at least be in global balance to within this amount, so that subtracting the imbalance from the local net heating would yield uncertainties of no more than ±0.1–0.2 K day^{-1}.

We have constructed a radiative transfer algorithm comprised of a carefully chosen collection of existing methods, which appears to satisfy our stated criterion of accuracy while remaining computationally efficient. We have paid particular attention to a proper treatment of the transition from pressure to Doppler broadening in the 15-micron band of carbon dioxide and the pure rotational band of water vapor, as well as on a more precise calculation of the infrared absorption by ozone (based on Rosenfield 1991). The first factor results in an improved horizontally averaged radiative balance in the upper stratosphere, whereas the second produces a lower net heating in the tropics, also resulting in a better balance in the lower stratosphere. The resulting net heating rates produce a weaker Brewer–Dobson circulation than do previous diagnostic studies.

In the process of evaluating our radiative code, we have demonstrated three important results. First, the exclusion of clouds in both the infrared and solar radiative algorithms does not significantly affect the net heating of the stratosphere, whereas treating cloudiness inconsistently does. Secondly, inadequate physical or numerical schemes tend to produce serious and intolerable errors in the calculated net heating of the tropical lower stratosphere; the most commonly used approximations and resolutions tend largely to overestimate the net positive heating in the tropical lower stratosphere by a factor of 2. Third, changes in radiative heating of 0.1–0.2 K day^{-1} in the lower stratosphere can significantly affect the global distribution of chemical tracers. These results must be taken into consideration in the design of future models of the stratosphere that incorporate radiative feedbacks.

Acknowledgments. We would like to thank Yuk Yang and David Crisp of Caltech, Joan Rosenfield of NASA, and Conway Leovy of the University of Washington for their helpful suggestions and comments. We also thank Stuart Freidenreich of Princeton for kindly providing us the GFDL LBL data.

This research was supported by NASA under Grants NAGW-910, NAGW-1605, and NAG-1-1404, and by NSF's Climate Dynamics Program under Grant ATM-8903340.

REFERENCES

Allen, M., and J. E. Frederick, 1982: Effective photodissociation cross sections for molecular oxygen and nitric oxide in the Schumann–Runge bands. *J. Atmos. Sci.*, **39**, 2066–2075.

Barnett, J. J., and M. Corney, 1985: Middle atmosphere reference model derived from satellite data. *Middle Atmosphere Program Handbook*, Vol. 16, K. Labitzke, J. J. Barnett, and B. Edwards, Eds., SCOSTEP Secretariat, University of Illinois, Urbana, Illinois, 47.

Brewer, A. M., 1949: Evidence for a world circulation provided by the measurements of helium and water vapor distributions in the stratosphere. *Quart. J. Roy. Meteor. Soc.*, **75**, 351–363.

Callis, L. B., R. E. Boughner, and J. D. Lambeth, 1987: The stratosphere: Climatologies of the radiative heating and cooling rates and the diabatically diagnosed net circulation fields. *J. Geophys. Res.*, **92**, 5585–5607.

Cess, R. D., 1976: Climate change: An appraisal of atmospheric feedback mechanisms employing zonal climatology. *J. Atmos. Sci.*, **33**, 1831–1843.

——, D. P., Kratz, S. J., Kim, and J. Caldwell, 1986: Infrared radiation models for atmospheric methane. *J. Geophys. Res.*, **91**, 9857–9864.

Chou, M. D., and L. Kouvaris, 1986: Atmospheric radiative transfer due to molecular line absorption, Part I: Monochromatic calculations. *J. Geophys. Res.*, **91**, 4047–4055.

Crisp, D., 1989: Comparison of thermal infrared cooling rates. *Two-Dimensional Intercomparison of Stratospheric Models*, C. H. Jackman, R. K. Seals, and M. J. Prather, Eds., NASA Conf. Pub. 3042, 89–107.

——, S. B. Fels, and M. D. Schwarzkopf, 1986: Approximate methods for finding CO_2 15-mm band transmission in planetary atmospheres. *J. Geophys. Res.*, **91**, 11 851–11 866.

Cunnold, D., F. Alyea, N. Phillips, and R. Prinn, 1975: A three-dimensional dynamical–chemical model of atmospheric ozone. *J. Atmos. Sci.*, **32**, 170–194.

Dobson, G. M. B., 1956: Origin and distribution of polyatomic molecules in the atmosphere. *Proc. Roy. Soc. London,* **A236,** 187–193.

Donner, L., and V. Ramanathan, 1980: Methane and nitrous oxide: Their effects on the terrestrial climate. *J. Atmos. Sci.,* **43,** 119–124.

Dunkerton, T. J., 1978: On the mean meridional mass motions of the stratosphere and mesosphere. *J. Atmos. Sci.,* **35,** 2325–2333.

Ellingson, R. G., and Y. Fouquart, 1991: The intercomparison of radiation codes in the climate models: An overview. *J. Geophys. Res.,* **96,** 8925–8927.

——, J. Ellis, and S. Fels, 1991: The intercomparison of radiation codes in the climate models: Long wave results. *J. Geophys. Res.,* **96,** 8929–8953.

Fels, S. B., 1979: Simple strategies for inclusion of Voigt effects in infrared cooling calculations. *Appl. Opt.,* **18,** 2634–2637.

——, and M. D. Schwarzkopf, 1975: The simplified exchange approximation: A new method for radiative transfer calculations. *J. Atmos. Sci.,* **32,** 1475–1488.

——, and ——, 1981: An efficient, accurate algorithm for calculating CO_2 15 mm band cooling rates. *J. Geophys. Res.,* **86,** 1205–1232.

Fleig, A. J., R. D. McPeters, P. K. Bhartia, B. M. Schlesinger, R. P. Cebula, K. F. Klenk, S. L. Taylor, and D. F. Heath, 1990: Nimbus 7 solar backscatter ultraviolet (SBUV) ozone products user's guide, NASA Ref. Publ., 1234, 19–25.

Gille, J. C., and L. V. Lyjak, 1986: Radiative heating and cooling rates in the middle atmosphere. *J. Atmos. Sci.,* **43,** 2215–2229.

——, J. M. Russell III, P. L. Bailey, L. L. Gordley, E. E. Remsberg, J. H. Lienesch, W. G. Planet, F. B. House, L. V. Lyjak, and S. A. Beck, 1984: Validation of the temperature retrievals obtained by the Limb Infrared Monitor of the Stratosphere (LIMS) experiment on *NIMBUS 7. J. Geophys. Res.,* **89,** 5147–5160.

——, L. V. Lyjak, and A. K. Smith, 1987: The residual circulation in the stratosphere. *J. Atmos. Sci.,* **44,** 1437–1452.

Goody, R., 1952: A statistical model for water vapor absorption. *J. Meteorol.,* **78,** 165–169.

Green, A. E. S., 1964: Attenuation by ozone and the earth's albedo in the middle ultraviolet. *Appl. Opt.,* **3,** 203.

Guthrie, P. D., C. H. Jackman, T. L. Kucsera, and J. E. Rosenfield, 1990: On the sensitivity of residual circulation model to differences in input temperature data, *J. Geophys. Res.,* **95,** 873–882.

Haigh, J. D., 1984: Radiative heating of the lower stratosphere and the distribution of ozone in a two-dimensional model. *Quart. J. Roy. Meteor. Soc.,* **110,** 167–189.

Harshvardhan, R. Davies, D. A. Randall, and T. G. Corsetti, 1987: A fast radiation parameterization for atmospheric circulation models. *J. Geophys. Res.,* **92,** 1009–1016.

Houghton, J. T., 1977: *The Physics of Atmospheres.* Cambridge University Press, 203 pp.

Jackman, C. H., R. S. Stolarski, and J. A. Kaye, 1986: Two-dimensional monthly average ozone balance from Limb Infrared Monitor of the Stratosphere and Stratospheric and Mesospheric Sounder data. *J. Geophys. Res.,* **91,** 1103–1116.

——, A. R. Douglass, P. D. Guthrie, and R. S. Stolarski, 1989: The sensitivity of total ozone and ozone perturbation scenarios in a two-dimensional model to dynamical inputs. *J. Geophys. Res.,* **94,** 9873–9887.

Jet Propulsion Laboratory, 1987: Chemical kinetics and photochemical data for use in stratospheric modeling. NASA Evaluation 8, JPL Publ. 87–41.

Joseph, J. H., W. J. Wiscombe, and J. A. Weinman, 1976: The delta-Eddington approximation for radiative flux transfer. *J. Atmos. Sci.,* **33,** 2452–2459.

Keating, G. M., and D. F. Young, 1985: Interim reference ozone models for the middle atmosphere. *Middle Atmosphere Program Handbook,* Vol. 16, K. Labitzke, J. J. Barnett, and B. Edwards, Eds., 205–229.

Kiehl, J. T., and S. Solomon, 1986: On the radiative balance of the stratosphere. *J. Atmos. Sci.,* **43,** 1525–1534.

——, C. Bruhl, and T. Yamanouchi, 1985: A parameterization for the absorption due to the near infrared bands of CO_2, *Tellus,* **37B,** 189.

——, R. J. Wolski, B. P. Briegleb, and V. Ramanathan, 1987: Documentation of radiation and cloud routines in the NCAR Community Climate Model. NCAR/TN-288+IA, National Center for Atmospheric Research, Boulder, CO, 109 pp.

King, M. D., and Harshvardhan, 1986: Comparative accuracy of selected multiple scattering approximations. *J. Atmos. Sci.,* **43,** 784–801.

Lacis, A. A., and J. E. Hansen, 1974: A parameterization for the absorption of solar radiation in the earth's atmosphere. *J. Atmos. Sci.,* **31,** 118–133.

Luther, F. M., and Y. Fouquart, 1984: The intercomparison of radiation codes used in climate models (ICRCCM). WMO Rep. WCP-93, 37 pp.

Malkmus, W., 1967: Random Lorentz band model with exponential-tailed S^{-1} line intensity distribution function. *J. Opt. Soc. Am.,* **57,** 323–329.

McClatchey, R. A., R. W. Fenn, J. E. A. Selby, F. E. Voltz, and J. S. Garing, 1971: Optical properties of the atmosphere (revised), Rep. AFCRL-71-0279, Air Force Cambridge Research Laboratory, Bedford, MA, 85 pp.

Murgatroyd, R. J., and F. Singleton, 1961: Possible meridional circulations in the stratosphere and mesosphere. *Quart. J. Roy. Meteor. Soc.,* **87,** 125–135.

Newell, R. E., J. W. Kidson, D. G. Vincent, and G. J. Boer, 1974: *The General Circulation of the Tropical Atmosphere and Interactions with Extratropical Latitudes,* Vol. 2, MIT Press, 370 pp.

Ou, S.-C. S., and K.-N. Liou, 1983: Parameterization of carbon dioxide 15 mm band absorption and emission. *J. Geophys. Res.,* **88,** 5203–5207.

Pawson, S., and R. S. Harwood, 1989: Monthly-mean diabatic circulations in the stratosphere. *Quart. J. Roy. Met. Soc.,* **115,** 807.

Ramanathan, V., 1976: Radiative transfer within the earth's troposphere and stratosphere: A simplified radiative convective model. *J. Atmos. Sci.,* **33,** 1330–1346.

——, and P. Downey, 1986: A nonisothermal emissivity and absorptivity formulation for water vapor. *J. Geophys. Res.,* **91,** 8649–8666.

Roberts, R. E., J. E. A. Selby, and L. M. Biberman, 1976: Infrared continuum absorption by atmospheric water vapor in the 8–12 mm window. *Appl. Opt.* **15,** 2085–2090.

Rodgers, C. D., 1967: The use of emissivity in atmospheric radiation calculations. *Quart. J. Roy. Meteor. Soc.,* **93,** 43.

——, 1968: Some extensions and applications of the new random model for molecular band transmission. *Quart. J. Roy. Meteor. Soc.,* **94,** 99–102.

——, and C. D. Walshaw, 1966: The computation of infra-red cooling rate in planetary atmospheres. *Quart. J. Roy. Meteor. Soc.,* **92,** 67–92.

——, and A. P. Williams, 1974: Integrated absorption of a spectral line with the Voigt profile. *J. Quant. Spectrosc. Radiat. Transfer,* **14,** 319.

Rosenfield, J. E., 1991: A simple parameterization of ozone infrared absorption for atmospheric heating rate calculations. *J. Geophys. Res.,* **96,** 9065–9074.

——, M. R. Schoeberl, and M. A. Geller, 1987: A computation of the stratospheric residual circulation using an accurate radiative transfer model. *J. Atmos. Sci.,* **44,** 859–876.

Rothman, L. S., R. R. Gamache, L. R. Brown, R. A. Toth, H. M. Pickett, R. L. Poynter, J. M. Flaud, C. Camy-Peyrey, A. Barbe, N. Husson, C. P. Rinsland, and M. A. H. Smith, 1987: The HITRAN database: 1986 edition. *Appl. Opt.,* **26,** 4058–4097.

Sasamori, T., J. London, and D. V. Hoyt, 1972: Radiation budget of the Southern Hemisphere. *Meteor. Monogr.,* **13,** No. 35, Amer. Meteor. Soc.

Schwarzkopf, M. D., and S. B. Fels, 1985: Improvements to the algorithm for computing CO_2 transmissivities and cooling rates. *J. Geophys. Res.,* **90,** 10 541–10 550.

——, and ——, 1991: The simplified exchange method revisited: An accurate, rapid method for computation of infrared cooling rates and fluxes. *J. Geophys. Res.*, **86,** 9075–9096.

Sellers, W. D., 1965: Physical climatology, 272 pp. University of Chicago Press, Chicago, IL.

Shia, R. L., Y. L. Yung, M. Allen, R. W. Zurek, and D. Crisp, 1989: Sensitivity study of advection and diffusion coefficients in a two-dimensional stratospheric model using excess carbon 14 data. *J. Geophys. Res.*, **94,** 18 467–18 484.

Solomon, S., J. T. Kiehl, R. R. García, and W. Grose, 1986: Tracer transport by the diabatic circulation deduced from satellite observations. *J. Atmos. Sci.*, **43,** 1603–1617.

Somerville, R. C. J., P. H. Stone, M. Halem, J. E. Hansen, J. S. Hogan, L. M. Druyan, G. Russell, A. A. Lacis, W. J. Quirk, and J. Tenenbaum, 1974: The GISS model of the global atmosphere. *J. Atmos. Sci.*, **31,** 84–117.

Stephens, G. L., 1984: The parameterization of radiation for numerical weather prediction and climate models. *Mon. Wea. Rev.*, **112,** 826–867.

Strobel, D. F., 1978: Parameterization of the atmospheric heating rate from 15 to 120 km due to O_2 and O_3 absorption of solar radiation. *J. Geophys. Res.*, **83,** 6225–6230.

Tung, K. K., 1982: On the two-dimensional transport of stratospheric trace gases in isentropic coordinates. *J. Atmos. Sci.*, **39,** 2330–2355.

——, 1986: Nongeostrophic theory of zonally averaged circulation. Part I: Formulation. *J. Atmos. Sci.*, **43,** 2600–2618.

Yang, H., K. K. Tung, and E. P. Olaguer, 1990: Nongeostrophic theory of zonally averaged circulation, Part II: Eliassen-Palm flux divergence and isentropic mixing coefficient. *J. Atmos. Sci.*, **47,** 215–241.

——, E. Olaguer, and K. K. Tung, 1991: Simulation of the present-day chemical composition of the stratosphere using a coupled 2D model in isentropic coordinates. *J. Atmos. Sci.*, **48,** 442–471.

Wehrbein, W. M., and C. B. Leovy, 1982: An accurate radiative heating and cooling algorithm for use in dynamical models of the middle atmosphere. *J. Atmos. Sci.*, **39,** 1532–1544.

World Meteorological Organization, 1982: Stratosphere 1981: Theory and Measurement. WMO Rep. 11, 516 pp.

——, 1986: Atmospheric ozone 1985: Assessment of our understanding of the processes controlling its present distribution and change. WMO Rep. 16, Global Ozone Res. and Monit. Proj.

Zhu, X., 1988: An improved Voigt line approximation for the calculation of equivalent width and transmission. *J. Quant. Spectrosc. Radiat. Transfer,* **39,** 421.